A Bicycle Can Be Self-Stable Without Gyroscopic or Caster Effects

J. D. G. Kooijman,[1] J. P. Meijaard,[2] Jim M. Papadopoulos,[3] Andy Ruina,[4]* A. L. Schwab[1]

A riderless bicycle can automatically steer itself so as to recover from falls. The common view is that this self-steering is caused by gyroscopic precession of the front wheel, or by the wheel contact trailing like a caster behind the steer axis. We show that neither effect is necessary for self-stability. Using linearized stability calculations as a guide, we built a bicycle with extra counter-rotating wheels (canceling the wheel spin angular momentum) and with its front-wheel ground-contact forward of the steer axis (making the trailing distance negative). When laterally disturbed from rolling straight, this bicycle automatically recovers to upright travel. Our results show that various design variables, like the front mass location and the steer axis tilt, contribute to stability in complex interacting ways.

A bicycle and rider in forward motion balance by steering toward a fall, which brings the wheels back under the rider [supporting online material (SOM) text S1 and S2] (*1*). Normally, riders turn the handlebars with their hands to steer for balance. With hands off the handlebars, body-leaning relative to the bicycle frame can also cause appropriate steering. Amazingly, many moving bicycles with no rider can steer themselves so as to balance—likewise with a rigid rider whose hands are off the handlebars. For example, in 1876, Spencer (*2*, *3*) noted that one could ride a bicycle while lying on the seat with hands off, and the film *Jour de Fête* by Jacques Tati, 1949, features a riderless bicycle self-balancing for long distances. Suspecting that bicycle rideability, with rider control, is correlated with self-stability of the passive bicycle, much theoretical research has focused on this bicycle self-stability.

The first analytic predictions of bicycle self-stability were presented independently by French mathematician Emmanuel Carvallo (1897) (*4*) and Cambridge undergraduate Francis Whipple (1899) (*3*, *5*). In their models and in this paper, a bicycle is defined as a three-dimensional mechanism (Fig. 1A) made up of four rigid objects (the rear frame with rider body B, the handlebar assembly H, and two rolling wheels R and F) connected by three hinges. The more complete Whipple version has 25 geometry and mass parameters. Assuming small lean and steer angles, linear and angular momentum balance—as constrained by the hinges and rolling contact—lead to a pair of coupled second-order linear differential equations for leaning and steering (SOM text S3) (*6*). Solutions of these equations show that after small perturbations, the motions of a bicycle may exponentially decay in time to upright straight-ahead motion (asymptotic stability). This stability typically can occur at forward speeds v near to $\sqrt{gL}$, where g is gravity and L is a characteristic length (about 1 m for a modern bicycle). Limitations in the model include assumed linearity and the neglect of motions associated with tire and frame deformation, tire slip, and play and friction in the hinges. Nonetheless, modern experiments have demonstrated the accuracy of the Whipple model for a real bicycle without a rider (*7*).

The simple bicycle model above is energy-conserving. Thus, the asymptotic stability of a bicycle, that the lean and steer angles exponentially decay to zero after a perturbation, is jarring to those familiar with Hamiltonian dynamics. But because of the rolling (non-holonomic) contact of the bicycle wheels, the bicycle—although energy-conserving—is not Hamiltonian, and it is possible for a subset of variables to have exponential stability in time (*6*, *8*). There is no contradiction between exponential decay and energy conservation because for a bicycle, the energy lost from decaying steering and leaning motions goes to increase the forward speed. Unresolved, however, is the cause of bicycle self-stability. In some sense, perhaps, a self-stable bicycle is something like a system with control, albeit self-imposed.

Rider-controlled stability of bicycles is indeed related to their self-stability. Experiments like those of Jones (*9*) and R. E. Klein (*10*) show that special experimental bicycles that are difficult for a person to ride, either with hands on or off, tend not to be self-stable. Both no-hands control (using body bending) and bicycle self-stability depend on "cross terms," in which leaning causes steering or vice versa. The central question about what causes self-stability is thus reduced to, what causes the appropriate coupling between leaning and steering? The most often discussed of the coupling effects are those due to front-wheel gyroscopic torque and to caster effects from the wheel trailing behind the steer axis. Trail (or "caster trail") is the distance c that the ground contact point trails behind the intersection of the steering axis with the ground (Fig. 1A).

There is near universal acceptance that either spin angular momentum (gyroscopic effect) or trail, or both, are necessary for bicycle self-stability (*3*). Active steering of a bicycle front wheel causes a gyroscopic torque on an upright frame and rider. Because the front wheel is relatively light as compared with the more massive bicycle and rider, the effect of this gyroscopic torque on the lean is generally small (SOM text S1) (*11*). However, coupling the other way—the effect of active bicycle-leaning on hands-free steering—is nonnegligible. For example, when the bicycle has a lean rate to the right the front axle also has a lean rate to the right, and the spinning wheel exerts a clockwise (looking down) reactive torque carried at least in part by the handlebar assembly. This reaction torque tends to turn the handlebars rightward. Thus, the common explanation of no-hands rider control: To steer to the right, the rider bends her upper body to the left, tilting the bicycle and wheels rightward (*5*). The bicycle

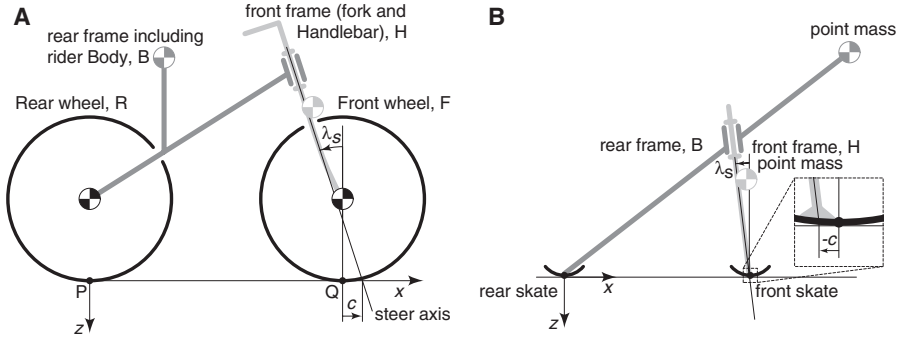

Fig. 1. (**A**) The bicycle model consists of two interconnected frames, B and H, connected to two wheels, R and F. The model has a total of 25 geometry and mass-distribution parameters. Central here are the rotary inertia I_{yy} of the front wheel, the steer axis angle ("rake") λ_s, and the trail distance c (positive if contact is behind the steer axis). Depending on the parameter values, as well as gravity g and forward speed v, this bicycle can be self-stable or not. (**B**) A theoretical TMS bicycle is a special case. It is described with only nine free parameters (eight plus trail). The wheels have no net rotary inertia and thus function effectively as ice skates. The two frames each have a single point mass and no mass moments of inertia. A heavy point mass on the rear skate at the ground contact point can prevent the bicycle from tipping over forward; because it has no effect on the linearized dynamics, it is not shown. Even with negative trail ($c < 0$; inset), this non-gyroscopic bicycle can be self-stable.

[1]Department of Mechanical Engineering, Delft University of Technology, Delft 2628 CD, Netherlands. [2]Department of Engineering Technology, University of Twente, Enschede 7500 AE, Netherlands. [3]Department of Engineering and Technology, University of Wisconsin–Stout, Menomonie, WI 54751, USA. [4]Department of Mechanical Engineering, Cornell University, Ithaca, NY 14853, USA.

*To whom correspondence should be addressed. E-mail: ruina@cornell.edu.

handlebars, considered as freely rotating on the steer axis and forced by the gyroscopic front wheel, thus initially turn rightward. Such leaning-induced steering can be used for rider control of balance. Likewise, this gyroscopic coupling also contributes to a forward-moving passive bicycle self-steering toward a fall (*12*).

The most thorough discussion of the necessity of gyroscopic coupling of leaning to steering for bicycle self-stability is in the bicycle chapter of the fourth volume of the gyroscope treatise by Klein and Sommerfeld (*11*, *13*). They took the example bicycle parameters from Whipple and eliminated just the spin angular momentum of the wheels. Using their own linearized dynamic stability analysis of the Whipple model, Klein and Sommerfeld concluded that, "... in the absence of gyroscopic actions, the speed range of complete stability would vanish" [(*11*) p. 866] and make what appears to be a strong general claim about bicycles: "The gyroscopic action, in spite of its smallness, is necessary for self-stability" [(*11*) p. 866].

They emphasized that the gyroscopic torque does not apply corrective lean torques to a bicycle directly, as others seem to have thought (*14*). Rather, through the gyroscopic torque, leaning causes steering, which in turn causes the righting accelerations: "The proper stabilizing force, which overwhelms the force of gravity, is the centrifugal force, and the gyroscopic action plays the role of a trigger" [(*11*) p. 881].

In Jones's famous search for an unrideable bicycle (URB) (*9*), he added a counter-rotating disk to the handlebar assembly, canceling the gyroscopic self-steering torque of the front wheel. He could still (barely) ride such a nongyro bicycle using no hands. Jones rightly deduced that the gyroscopic effect discussed in (*11*) was not the only coupling between leaning and steering. Jones emphasized the importance of the front-wheel ground contact being behind the steering axis (positive trail, $c > 0$) (Fig. 1A). Even though the front forks of modern bicycles are typically bent forward slightly, with the wheel-center forward of the steering axis, all modern bicycles still have positive trail (typically from 2 to 10 cm on modern bicycles) because of the steering axis tilt $\lambda_s > 0$. When Jones modified his bicycle by placing the front-wheel ground contact in front of the steer axis (negative trail, $c < 0$), he could not ride using no hands.

In Jones's view, a bicycle wheel is in part like a caster wheel on a shopping cart, with the wheel trailing behind a vertical pivot axis. If a modern bicycle was rolled forward by guiding the rear frame in a straight line while it was held rigidly upright, the front wheel would quickly self-center like a shopping-cart caster. Jones noted, "The bicycle has only geometrical castor [sic] [trail] stability to provide its self-centering" [(*9*) p. 40]. Jones's main focus was a second trail effect: The vertical ground contact force on the front-wheel–ground contact point exerts a steering torque on a leaned bicycle even when the bicycle is steered straight. Jones calculated the steer torque caused by lean as a derivative of a static potential energy, neglecting the weight of the front assembly. If a typical modern bicycle is firmly held by the rear frame, leaned to the right, and pressed down hard, then the vertical ground contact force on the front wheel causes a rightward steering torque on the handlebars. The Jones torque can be felt on a normal bicycle by riding in a straight line and bending your upper body to the left, leaning the bicycle to the right: To maintain a straight path, the hands must fight the Jones torque and apply a leftward torque to the handlebars. According to Jones, this torque causes steering toward a fall only when the trail is positive. When the trail is zero, Jones's theory predicts no self-correcting steer torque. Jones seems to conclude that no-hands control authority (the ability to cause steering by body bending) and self-stability both depend on positive trail. A mixture of the two mechanisms Jones discusses certainly suggests that trail is a key part of bicycle stability.

Following Klein and Sommerfeld and Jones, it has become common belief that steering is stable because the front-wheel–ground contact drags behind the steering axis, and leaning is stable because some mixture of gyroscopic torques and trail causes an uncontrolled bicycle to steer in the direction of a fall (*3*).

Are gyroscopic terms or positive trail, together or separately, really either necessary or sufficient for bicycle self-stability? Following Carvallo, Whipple, Klein and Sommerfeld, and others since [see history in (*6*)], we began with the linearized equations of motion. Using the numerical values from the benchmark example in (*6*) and setting the gyroscopic terms to zero, we found that self-stability is lost (SOM text S6.1, which is similar to the result of Klein and Sommerfeld for the Whipple parameters). However, we also found bicycle designs that are self-stable even without gyroscopic terms.

The conflict with Klein and Sommerfeld is partly resolved by noting sign errors in their key stability term (*3*). Despite their calculation errors, the Whipple bicycle with Whipple's example parameters does indeed lose self-stability when the gyro terms are set to zero. But with their incorrect expressions, Klein and Sommerfeld could make slightly more general claims that are not valid when the sign errors are corrected (*3*). Whatever generality Klein and Sommerfeld intended (their wording is ambiguous), their result does not apply to bicycles in general.

Similarly, Jones's simplified static-energy calculation seems incomplete in the context of a dynamical system, such as the Whipple and Carvallo models. Jones's static energy calculation only calculates (incompletely) one term, $K_{0\delta\phi}$, of the full dynamics equations (*3*, *6*). In a full dynamic analysis, $K_{0\delta\phi}$ does not predict the steering of a falling bicycle (*3*). For example, that term can be nonzero for a bicycle that falls with no self-corrective steering at all. And just as for the gy-

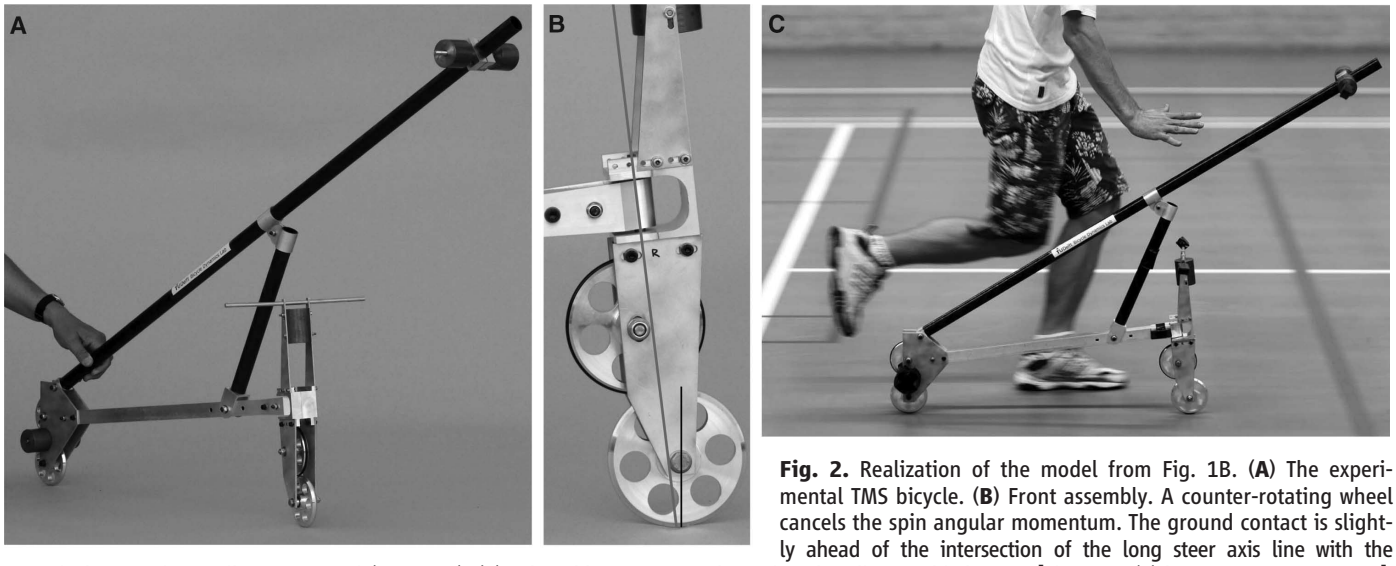

Fig. 2. Realization of the model from Fig. 1B. (**A**) The experimental TMS bicycle. (**B**) Front assembly. A counter-rotating wheel cancels the spin angular momentum. The ground contact is slightly ahead of the intersection of the long steer axis line with the ground, showing the small negative trail (movie S3). (**C**) Self-stable experimental TMS bicycle rolling and balancing [photo for (C) by S. Rentmeester/FMAX].

roscopic term, we can find designs with zero or negative trail that we predict are self-stable (SOM text S6.2).

In contrast to the conventional claims above for the necessity of gyroscopic terms and trail, we have found no rigorous reasoning that demands either. To understand better what is needed for self-stability, we eliminated as many bicycle parameters as possible (*15*). Most centrally, we eliminated the gyroscopic terms and set the trail to zero ($c = 0$). We also reduced the mass distribution to just two point masses: one for the rear frame B and one for the steering assembly H (Fig. 1B). With these theoretical parameters, the wheels—having no net spin angular momentum—are mechanically equivalent to skates. These simplifications reduce the number of parameters from Whipple's 25 to a more manageable eight.

Stability analysis of this theoretical two-mass-skate (TMS) bicycle model (SOM text S7), confirmed by means of numerical solution of the governing differential equations, shows that neither gyroscopic terms nor positive trail are needed for self-stability [Routh-Hurwitz analysis shows that all eigenvalues of the theoretical TMS bicycle can have negative real parts at some forward speeds (*16*)].

We used the stable theoretical TMS bicycle parameters as a basis for building an experimental TMS bicycle (Fig. 2A and SOM text S8 and S9). We used small wheels to minimize the spin angular momentum. To further reduce the gyroscopic terms, following Jones we added counter-spinning disks that rotate backward relative to the lower wheels (Fig. 2B and movie S2). The experimental TMS bicycle was built to have a slightly negative trail ($c = -4$ mm < 0) (movie S3). Although the experimental TMS bicycle looks like a folding scooter, it is still a bicycle (two wheels, two frames, and three hinges).

Because all physical objects have distributed mass, the measured parameters of the experimental TMS bicycle were necessarily slightly different from those of the theoretical design, which was based on point masses. Using measured parameters, we calculated the stability plot of Fig. 3A (SOM text S7 and S8). For rolling speeds greater than 2.3 m/s, all eigenvalues have negative real parts (implying self-stability).

After an initial forward push, the coasting experimental TMS bicycle (Fig. 2C) would remain upright before it slowed down to about 2 m/s (SOM text S10 and S11 and movie S1). As it slowed below 2 m/s, the bicycle would begin to fall. In a perturbation experiment, the stable coasting bicycle ($v > 2.3$ m/s) was hit sideways on the frame, causing a jump in the lean rate, followed by a recovery to straight-ahead upright rolling.

The lean and yaw rates were measured (telemetered). A data set was compared with theory in Fig. 3B (movie S4). One difference between experiment and theory is lateral wheel slip at the initial perturbation, which caused an initial jump in the measured yaw rate (Fig. 3B, triangles in the first 0.25 s). The theoretical model assumed no slip. High-speed video (movie S4) also shows a 20-Hz shimmy, which is due at least in part to unmodeled steering axis play (SOM text S11). Nonetheless, after the slipping period—even with the shimmy—the data reasonably track the low-dimensional linear model's predictions.

Both the theoretical analysis and physical experiment show that neither gyroscopic torques nor trail are necessary for bicycle self-stability. Nor are they sufficient. Many bicycle designs with gyroscopic front wheels and positive trail are unstable at every forward speed (SOM text S6.3). Also, all known bicycle and motorcycle designs lose self-stability at high speeds because of gyroscopic terms [for example, (*6*)]. In contrast, the TMS bicycle does not have gyroscopic terms and is predicted to maintain stability at high speeds.

With no gyroscopic torque and no trail, why does our experimental TMS bicycle turn in the direction of a fall? A general bicycle is complicated, with various terms that can cause the needed coupling of leaning to steering. Only some of these terms depend on positive trail or on positive spin angular momentum in the front wheel. In the theoretical and experimental TMS designs, the front assembly mass is forward of the steering axis and lower than the rear-frame mass. When the TMS bicycle falls, the lower steering-mass would, on its own, fall faster than the higher frame-mass for the same reason that a short pencil balanced on end (an inverted pendulum) falls faster than a tall broomstick (a slower inverted pendulum). Because the frames are hinged together, the tendency for the front steering-assembly mass to fall faster causes steering in the fall direction. The importance of front assembly mass for Jones-like static torques has been noted before (*8*, *17*, *18*).

Why does this bicycle steer the proper amounts at the proper times to assure self-stability? We have found no simple physical explanation equivalent to the mathematical statement that all eigenvalues must have negative real parts (SOM text S4). For example, turning toward a fall is not sufficient to guarantee self-stability. For various candidate simple sufficient conditions X for stability, we have found designs that have X but that are not self-stable. For example, we have found bicycles with gyroscopic wheels and positive trail that are not stable at any speed (SOM text S6.3). We also have found no simple necessary conditions for self-stability. Besides the TMS design with no gyroscope and negative trail, we have found other counterexamples to common lore. We have found a bicycle that is self-stable with rear-wheel steering (SOM text S6.7). We also found an alternative theoretical TMS design that has, in addition to no-gyro and negative trail, also a negative head angle ($\lambda_s < 0$) (SOM text S6.6).

Are there any simply described design features that are univerally needed for bicycle self-stability? Within the domain of our linearized equations, we have found one simple necessary condition (SOM text S5): To hold a self-stable bicycle in a right steady turn requires a left torque on the handlebars. Equivalently, if the hands are suddenly released from holding a self-stable bicycle in a steady turn to the right, the immediate first motion of the handlebars will be a turn further to the right. This is a rigorous version of the more general, as-yet-unproved claim that a stable bicycle must turn toward a fall.

Another simple necessary condition for self-stability is that at least one factor coupling lean to steer must be present [at least one of $M_{\delta\phi}$, $C_{\delta\phi}$, or $K_{\delta\phi}$ must be nonzero (SOM text S3)]. These coupling terms arise from combinations of trail,

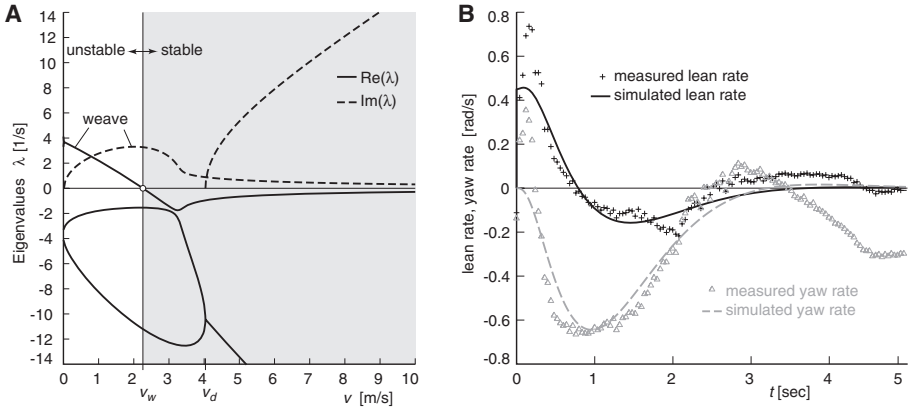

Fig. 3. (**A**) Stability plot for the experimental TMS stable bicycle. Solutions of the differential equations are exponential functions of time. Stability corresponds to all such solutions having exponential decay (rather than exponential growth). Such decay only occurs if all four of the eigenvalues λ_i (which are generally complex numbers) have negative real parts. The plot shows calculated eigenvalues as a function of forward speed v. For $v > 2.3$ m/s (the shaded region), the real parts (solid lines) of all eigenvalues are negative (below the horizontal axis), and the bicycle is self-stable. (**B**) Transient motion after a disturbance for the experimental TMS bicycle. Measured and predicted lean and yaw (heading) rates of the rear frame are shown. The predicted motions show the theoretical (oscillatory) exponential decay. Not visible in these plots, but visible in high-speed video (movie S4), is a 20-Hz shimmy that is not predicted by the low-dimensional linearized model (SOM text S10 and S11).

spin momentum, steer axis tilt, and center of mass locations and products of inertia of the front and rear assemblies.

Although we showed that neither front-wheel spin angular momentum nor trail are necessary for self-stability, we do not deny that both are often important contributors. But other parameters are also important, especially the front-assembly mass distribution, and all of the parameters interact in complex ways. As a rule, we have found that almost any self-stable bicycle can be made unstable by misadjusting only the trail, or only the front-wheel gyro, or only the front-assembly center-of-mass position. Conversely, many unstable bicycles can be made stable by appropriately adjusting any one of these three design variables, sometimes in an unusual way. These results hint that the evolutionary, and generally incremental, process that has led to common present bicycle designs might not yet have explored potentially useful regions in design space.

References and Notes

1. W. J. M. Rankine, *The Engineer* **28**, 79 (in five parts) (1869).
2. C. Spencer, *The Modern Bicycle* (Frederick Warne and Co., London, 1876), pp. 23–24.
3. J. P. Meijaard, J. M. Papadopoulos, A. Ruina, A. L. Schwab, http://ecommons.library.cornell.edu/handle/1813/22497 (2011).
4. E. Carvallo, *Théorie du Mouvement du Monocycle et de la Bicyclette* (Gauthier-Villars, Paris, France, 1899).
5. F. J. W. Whipple, *Quarterly Journal of Pure and Applied Mathematics* **30**, 312 (1899).
6. J. P. Meijaard, J. M. Papadopoulos, A. Ruina, A. L. Schwab, *Proc. R. Soc. Lond. A* **463**, 1955 (2007).
7. J. D. G. Kooijman, A. L. Schwab, J. P. Meijaard, *Multibody Syst. Dyn.* **19**, 115 (2008).
8. J. I. Neĭmark, N. A. Fufaev, *Dynamics of Nonholonomic Systems* (Nauka, Moscow, 1967) [J. R. Barbour, transl. (American Mathematical Society, Providence, RI, 1972)].
9. D. E. H. Jones, *Phys. Today* **23**, 34 (1970) [reprinted by *Phys. Today* **59**, 9 (2006), pp. 51–56].
10. K. J. Åström, R. E. Klein, A. Lennartsson, *IEEE Contr. Syst. Mag.* **25**, 26 (2005).
11. F. Klein, A. Sommerfeld, *Über die Theorie des Kreisels* (Teubner, Leipzig, 1910).
12. J. A. Griffiths, *Proc. Inst. Mech. Eng.* **37**, 128 (1886).
13. In the preface to (*11*), the authors credit Fritz Noether for the ideas in the bicycle chapter.
14. W. Thomson, *Popular Lectures and Addresses* (Macmillian, London, 1889), **1**, pp. 142–146.
15. J. M. Papadopoulos, Bicycle steering dynamics and self-stability: A summary report on work in progress (1987), Internal report from the Cornell Bicycle Research Project; available at http://ruina.tam.cornell.edu/research/topics/bicycle_mechanics/bicycle_steering.pdf.
16. E. J. Routh, *Proc. Lond. Math. Soc.* **1**, 97 (1873).
17. R. N. Collins, thesis, University of Wisconsin, Madison, WI (1963).
18. C. Chateau, *La Nature* **20**, 353 (1892).

19. R. S. Hand helped with the theory and experiments; A. Dressel helped with the eigenvalue analysis; J. van Frankenhuyzen helped with designing the experimental machine; and J. Moore helped with conducting the experiments. The manuscript was improved by comments from M. Broide, M. Cook, A. Dressel, J. Guckenheimer, R. Klein, D. Limebeer, C. Miller, J. Moore, R. Pohl, L. Schaffer, and D. van Nouhuys. The research was initially supported by a NSF Presidential Young Investigators award to A.R. The original theory was mostly by J.M.P. with later refinement by A.L.S. J.P.M. found the error in (*11*). Experiments were performed mostly by J.D.G.K. and A.L.S. Writing was done mostly by A.R. and A.L.S.

Supporting Online Material

www.sciencemag.org/cgi/content/full/332/6027/339/DC1
Materials and Methods
SOM Text S1 to S11
Figs. S1 to S19
Tables S1 to S4
References
Movies S1 to S4

20 December 2010; accepted 10 March 2011
10.1126/science.1201959

DNA Origami with Complex Curvatures in Three-Dimensional Space

Dongran Han,[1,2]* Suchetan Pal,[1,2] Jeanette Nangreave,[1,2] Zhengtao Deng,[1,2] Yan Liu,[1,2]* Hao Yan[1,2]*

We present a strategy to design and construct self-assembling DNA nanostructures that define intricate curved surfaces in three-dimensional (3D) space using the DNA origami folding technique. Double-helical DNA is bent to follow the rounded contours of the target object, and potential strand crossovers are subsequently identified. Concentric rings of DNA are used to generate in-plane curvature, constrained to 2D by rationally designed geometries and crossover networks. Out-of-plane curvature is introduced by adjusting the particular position and pattern of crossovers between adjacent DNA double helices, whose conformation often deviates from the natural, B-form twist density. A series of DNA nanostructures with high curvature—such as 2D arrangements of concentric rings and 3D spherical shells, ellipsoidal shells, and a nanoflask—were assembled.

DNA nanotechnology can now be used to assemble nanoscale structures with a variety of geometric shapes (*1*–*12*) [for a recent review, see (*13*)]. Conventionally, a series of B-form double helices are brought together and arranged with their helical axes parallel to one another. The structure is held together by crossovers between neighboring helices, and the allowed crossover points are based on the pre-existing structural characteristics of B-form DNA. Many DNA nanostructures are variations of polygonal shapes and, although this level of complexity has been sufficient for many purposes, it remains a challenge to mimic the elaborate geometries in nature because most biological molecules have globular shapes that contain intricate three-dimensional (3D) curves. Here, we reveal a DNA origami design strategy to engineer complex, arbitrarily shaped 3D DNA nanostructures that have substantial intrinsic curvatures. Our approach does not require strict adherence to conventional design "rules" but instead involves careful consideration of the ideal placement of crossovers and nick points into a conceptually prearranged scaffold to provide a combination of structural flexibility and stability.

The scaffolded DNA origami folding technique, in which numerous short single strands of DNA (staples) are used to direct the folding of a long single strand of DNA (scaffold), is thus far one of the most successful construction methods based on parallel, B-form DNA (*14*). The most commonly used scaffold (M13) is ~7000 nucleotides (nts) long and is routinely used to construct objects with tens to hundreds of nanometer dimensions. Several basic, geometric 3D shapes such as hollow polygons and densely packed cuboids have been demonstrated, as well as a few examples of more complex structures, including a railed bridge and slotted or stacked crosses (*15*–*17*). The biggest limitation with conventional, block-based DNA origami designs is the level of detail that can be achieved. Analogous to digitally encoded images, DNA origami structures are usually organized in a finite, raster grid, with each square/rectangular unit cell within the grid (pixel) corresponding to a certain length of double-helical DNA. The target shape is achieved by populating the grid with a discrete number of DNA pixels (for most origami structures, each DNA pixel has a parallel orientation with respect to the other pixels) in a pattern that generates the details and curves of the shape. However, as with all finite pixel-based techniques, rounded elements are approximated and intricate details are often lost.

Recently, Shih and co-workers reported an elegant strategy to design and construct relatively complex 3D DNA origami nanostructures that contain various degrees of twist and curvatures (*18*). This strategy uses targeted insertion and deletion of base pairs (bps) in selected segments within a 3D building block (a tightly cross-linked bundle of helices) to induce the desired curvature. Nevertheless, it remains a daunting task to engineer subtle curvatures on a 3D surface. Our goal is to develop design principles that will allow researchers to model arbitrary 3D shapes with control over the degree of surface curvature. In an escape from a rigid lattice model, our versatile strategy begins by defining the desired surface features of a target object with the scaf-

[1]The Biodesign Institute, Arizona State University, Tempe, AZ 85287, USA. [2]Department of Chemistry and Biochemistry, Arizona State University, Tempe, AZ 85287, USA.

*To whom correspondence should be addressed. E-mail: hao.yan@asu.edu (H.Y.); dongran.han@asu.edu (D.H.); yan_liu@asu.edu (Y.L.)

www.sciencemag.org/cgi/content/full/332/6027/339/DC1

Supporting Online Material for

A Bicycle Can Be Self-Stable Without Gyroscopic or Caster Effects

J. D. G. Kooijman, J. P. Meijaard, Jim M. Papadopoulos, Andy Ruina,* A. L. Schwab

*To whom correspondence should be addressed. E-mail: ruina@cornell.edu

Published 15 April 2011, *Science* **332**, 339 (2010)
DOI: 10.1126/science.1201959

This PDF file includes:

Other Supporting Online Material for this manuscript includes the following:
(available at www.sciencemag.org/cgi/content/full/332/6027/339/DC1)

Movies S1 to S4

Supporting Online Text Material (SOM Chapters 1-11)

for

A bicycle can be self-stable without gyroscopic or caster effects

Science Magazine, Vol. 332 no. 6027 pp. 339-342, April 15, 2011

J. D. G. Kooijman[1], J. P. Meijaard[2], Jim M. Papadopoulos[3],
Andy Ruina[4] & A. L. Schwab[1]

[1]Delft University of Technology, Delft, The Netherlands, a.l.schwab@tudelft.nl

[2]University of Twente, Enschede, The Netherlands

[3]UW-Stout, Menomonie, WI 54751, USA

[4]Cornell University, Ithaca, NY 14853, USA, ruina@cornell.edu

See also
History of thoughts about bicycle self-stability
by
Meijaard, Papadopoulos, Ruina & Schwab,
published simultaneously with this paper as a motivating document on
ecommons@cornell (April 14, 2011): http://hdl.handle.net/1813/22497.

Besides the videos on the Science Magazine website,
more and better quality videos and pictures can be found at:
http://bicycle.tudelft.nl/stablebicycle/
mirrored at
http://ruina.cornell.edu/research/bicycles/stablebicycle/

This draft: April 15, 2011

Summary

This Supplementary Online Material (SOM text Chapters 1-11), supports many of the claims in the main paper. This supplementary text is divided into two mostly-independent sections within which some of the chapters are also independent. The chapters are called out in the main paper. We end with a guide to the SOM videos. For those pursuing this supplement on its own, here is a summary.

Part I: Bicycle Self-Stability. We begin with a general discussion of which forces could and do right a falling bicycle with or without control (Chapter 1). For those interested in the nature of the control, we qualitatively explain the contributions of steering angle and of steering rate, (Chapter 2). The new results in this paper were discovered by investigating the equations of motion described in Meijaard *et al.* [6] (Chapter 3). Like others before us, we use the Routh stability criteria to examine the negativity of the real parts of the roots of the characteristic polynomial (Chapter 4). Some general features of the roots are noted, including the only simple necessary condition for self-stability that we know (Chapter 5). Besides the TMS bicycle which we built and tested, using the same equations we have also found a variety of other designs that, in theory, highlight one or another counterexample to common bicycle stability conjectures concerning gyros, trail, head angle and rear-wheel steering (Chapter 6).

Part II: Experimental design and testing. We begin by considering a highly simplified version of the general Whipple bicycle. This theoretical TMS bicycle is the core of the results in this paper (Chapter 7). There are various complications in reducing the point-mass concepts to a manufacturable design (Chapter 8), and then still more issues when building the machine (Chapter 9). The experiments are then described (Chapter 10). However, anyone attempting to reproduce the experiments should be aware of various experimental subtleties (Chapter 11).

Contents

Part I

BICYCLE SELF-STABILITY

Chapter 1

Forces that can right a bicycle

The focus of the main paper and this supplement is self-stability, the ability of a riderless bicycle to balance itself, that is, to automatically return to upright straight-ahead motion after a small disturbance. Self-stability also applies to a bicycle with a no-hands rigid rider. Before discussing self-stability in more detail, in this first chapter we review some general considerations about what can and does cause a bicycle (that may or may not have rider control) to lean in wanted and unwanted ways.

A bicycle is balanced in straight-ahead motion when the rider is over the wheels, that is, when the center of mass of the bicycle-rider system is directly over the support line which connects the points where the front and rear wheels touch the ground. Like an inverted pendulum, the more a bicycle leans away from this balance, the more gravity pulls it further. What forces counteract the destabilizing gravitational torques? What regulates or causes these stabilizing forces [18]? We discuss these questions below. They eventually lead to the more focused question; what causes automatic self-balancing steering of an uncontrolled bicycle?

The material reviewed in this chapter is almost entirely not original, but there is no simple reference for it.

What forces right a bicycle?

One can imagine several forces that might help to bring a falling bicycle upright. First let's name the dominant mechanism for forward-moving bicycles of common design.

As Rankine [1] noted in 1869, a forward-moving leaned bicycle is primarily righted by the lateral acceleration of the support line due to steering. To balance a bicycle that initially is falling to the left, it is steered to the left, causing the wheels to move on curved paths to the left. These leftward curved paths lead to a leftward acceleration of the support line. So a bicycle is balanced like an inverted broomstick is balanced on an open hand, by acceleration of the support back under the center of mass. To maneuver, riders manipulate this falling: to turn right they first counter-steer left, inducing a lean to the right, and then later steer right in the direction of the induced fall (see Figure 5 in Rankine [1], p. 153). More details concerning the lateral acceleration of the support line are in Chapter 2 below. Using these ideas it is, in principle, easy to steer and balance a bicycle [19] (although exactly how people actually do it is an open question [20, 21, 22]).

Acceleration of the support line, a clarification. When we discuss the acceleration of the ground support line of a forward moving bicycle, we are not talking about the acceleration of material points. At any instant in time there are two points where the front and rear wheels touch the ground. Those points define a line. We are talking about the acceleration of that line (and not the acceleration of the bits of rubber on the tires or the non-acceleration of the bits of pavement on

the ground). Alternatively, at any instant in time we can imagine rigid extensions of the rear and front frames that have on them points that instantaneously coincide with the ground contact points. It is the accelerations of those imaginary material points that concern us.

What forces do not right a bicycle?

First let's dismiss one gyroscopic effect. When a bicycle with fixed straight-ahead steering falls there are reaction torques on the frame and handlebars from the precession of the spinning wheels. However, these torques are orthogonal to the axis of fall and, for a bicycle with steering locked-straight ahead, are completely reacted by the moment from the lateral forces of the ground on the wheels. A bicycle with locked steering falls over when moving forward exactly as it does when not rolling: "any kind of gyroscopic stabilization is going to disappear" [11].

A second small gyroscopic effect is sometimes overstated: actively steering the relatively lighter spinning front wheel causes a forced-precession gyroscopic torque on the relatively heavier frame and rider. In order to conserve angular momentum a bicycle with spinning wheels floating in space would indeed tip right when steered left. (You can feel this leaning torque by holding a spinning bicycle wheel, with one hand on each end of the axle, and turning in place.) This term might be important on a special bicycle with a big gyrostat added to the front wheel. But for a typical bicycle, righting due to this gyroscopic torque is swamped by the support-line acceleration described above [18, 11].

A variety of other forces might contribute to righting a bicycle, some of them acting even at zero forward speed. Despite common lay confusions, and like the gyroscopic mechanisms discussed above, there is no controversy in the scientific literature about the general insignificance of all of these mechanisms to a typical bicycle's balance [18].

These further mechanisms (or effects), below, can move the center of mass and support line relative to each other, just not very much. There is no universal way of quantifying the importance of these effects; they are not generally associated with terms that can be set to zero without affecting others; the relative importance of the mechanism depends on whether steering is by a controlled torque or a controlled angle; and a small effect in one bicycle might be a large term in an unusual bicycle design. Finally, the contribution of an effect or term depends on the definition: contribution to *what*?

A candidate quantification is through a measure of control authority. For example, what is the largest lean angle from which a fall can be prevented with the proposed mechanism alone? But even then one needs to set bounds on the allowed angles of steer, allowed steer rates, allowed body bends, etc.

Here are six other effects that might be imagined to contribute to the righting of a falling bicycle, either by causing a lateral force on the center of mass, or by moving the support line, or both. We feel all of these are generally insignificant. All of these apply to a bicycle at, or close to rest, as much or more than they apply to a forward moving bicycle.

1. Because bicycle wheels are toroidal, and not knife-edged, tipping a bicycle rolls the ground contact sideways. Special training bicycles [10] with *very* broad wheels can be statically stable. Such bicycles have tire crown radius that is larger than the center-of-mass height. However, a standard bicycle, with tire radius a small fraction of the wheel radius, the contact point only moves a negligible few milimeters for a 10 degree lean.

2. Bending the rider's body causes a sideways ground reaction force that accelerates the system center of mass laterally. For a typical bicycle, leaning the body left relative to the frame causes a leftward force of the wheels on the ground, leading to a rightward acceleration of the center of mass. For example, a double pendulum can be balanced by an actuator at the

intermediate joint [23]. However, the system center of mass can only be moved a small distance by this means. The mechanism is the same as that used in tightrope walking (with no pole), but more difficult because of the more limited body motion and because of the mass distribution on a bicycle. Circus-level performers can wiggle their bodies so as to balance a stationary bicycle that is steered straight forward (as seen in YouTube videos of people riding bicycles along fence tops). When a bicycle is rolling forward without steering, this double-pendulum balance mechanism has no more or less ability to move the center of mass laterally than when it is stationary.

3. With the front wheel both steered substantially (say $90°$ to get the picture) and locked, tipping the bicycle rolls the front contact laterally. This is a partial contributor to the balance in a so-called 'track stand'. However, for typical bicycle layouts (with nearly vertical head angles), the system center of mass would have to be below a line connecting the rear wheel contact with a point somewhat above the center of the front wheel in order to get static stability this way.

4. With a large steering angle (say $45°$), rolling the rear wheel fore and aft moves the front contact laterally. This is the main balancing mechanism in a track stand: with the handlebar turned to the left, the rider pedals forward and backward to move the front support to the left and right, respectively. This mechanism depends on both forward acceleration and steer angle. It could contribute to balance during braking with large steering angles or during acceleration with large steer angles, but seems of little importance in normal riding where both forward acceleration and the steer angle are small.

5. Because for most bicycles the front wheel contact is not on the steering axis, steering a bicycle at rest causes a lateral motion of the frame. For a single point-mass bicycle and rider (with no steering assembly mass) this causes no acceleration of either the center of mass or the contact support points. For a distributed mass bicycle-rider system this can cause a small lateral force that laterally accelerates the center of mass.

6. Finally, if the steer-assembly has mass, steering can induce lateral ground reaction forces which laterally accelerate the center of mass. This is a similar mechanism to 2 above, but with the steer assembly replacing the upper-body bending. Few, if any, people can balance a conventional bicycle that is not rolling forward using steering-alone to balance.

In summary, the lean angle of a bicycle is affected by two dominant terms: 1) a destabilizing gravity torque (like the falling of an upside-down broom stick when initially balanced on end) and 2) the linear and angular acceleration of the support line due to steering angle and steering rate. Other effects are generally negligible.

Chapter 2

Both steering angle and steering rate cause lateral acceleration of the support line

The lateral acceleration of the support-line of a moving bicycle has contributions from both steering angle and steering angular rate.

To better understand these contributions, consider some *unusual* bicycles and skateboards, all of which have the simplification that the trail is zero for both front and rear wheels. For simplicity of discussion let's consider the lateral acceleration $a_{\rm M}$ of a point M which is midway between the front and rear wheels and on the ground.

Both-wheels steering. On a both-wheels-steer bicycle, where the rear wheel is steered as much but opposite to the front wheel M has a lateral acceleration due to the steer-angle but not due to the steer-rate [24].

$$a_{\rm M} = c_1\delta \qquad \text{(acceleration proportional to steer angle)} \tag{2.1}$$

Such a bicycle is said to be more difficult to ride [25]. This is somewhat like a conventional skateboard where the rear truck steers exactly opposite to the front truck (a'truck' is an assembly of two wheels, with steering mechanism, that is bolted to the bottom of the skateboard). On such a conventional skateboard M has only lateral acceleration due to the steer-angle [26].

Parallel steering. On the other hand, a bicycle with the rear wheel steered parallel to the front wheel, would have lateral acceleration of M due to steer-rate, but not due to steer-angle,

$$a_{\rm M} = c_2\dot{\delta} \qquad \text{(acceleration proportional to steer angle)} \tag{2.2}$$

Such a bicycle is easily balanced [25] (but can't be turned). This is like a modified skateboard with the rear truck made to steer parallel to the front truck, and thus having lateral acceleration due only to steer-rate. In a 15 minute experiment one can verify that such a parallel-steer skateboard can be easily balanced (but like a parallel-steered bicycle, can't be turned).

Combination. A conventional bicycle is between the two extremes of opposite and parallel steering, so both steer and steer rate contribute to the lateral acceleration of M. The curvature of the rear-wheel path is proportional to the steer angle: the bigger the steer angle the smaller the radius of the circle of the rear wheel path. And the path of the front wheel is additionally curved due to the rate of steering (i.e., the angular velocity of the handlebars relative to the frame). Even when passing through a steer angle of zero the steer rate causes a curved path of the front wheel (Rankine's 'promptitude' [1], 1870 p. 2). The acceleration of the midpoint M is the average of these front and rear wheel lateral accelerations.

$$a_{\rm M} = c_1\delta + c_2\dot{\delta} \tag{2.3}$$

Rear-wheel steering. On a backward-moving bicycle, or equivalently a reer-wheel-steered bicycle, steer and steer rate contribute with opposite signs,

$$a_{\mathrm{M}} = c_1\delta - c_2\dot{\delta}, \tag{2.4}$$

generally making such a bicycle more difficult to balance [1] (these rear-wheel-steer issues can be circumvented by adjusting the mass distribution, however [27]; see also Section 6.7).

Chapter 3

Review of the linearized equations of motion for the bicycle model

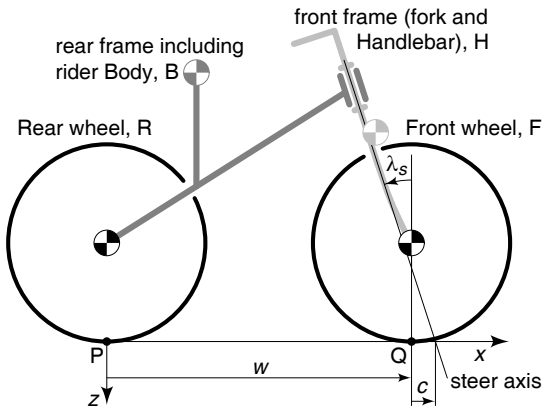

Figure 3.1: The Whipple bicycle model is described with 25 geometry and mass parameters. There are two frames B (rear frame plus rider Body) and H (fork plus Handlebar) connecting two wheels R (Rear) and F (Front). Each has geometric and mass parameters. The velocity degrees of freedom are the forward speed v, the rear frame lean rate $\dot{\phi}$ (positive for a rightward fall) and steer rate $\dot{\delta}$ (positive for a rightward turn). The steer axis tilt $\lambda_{\rm s}$, and trail c, are positive, as shown, on conventional bicycles. (Note that the eigenvalues λ_i, discussed in later chapters, are unrelated to the geometry parameter $\lambda_{\rm s}$.)

The bicycle model we use is the so-called Whipple [5] model described in Meijaard *et al.* [6] The model (see Figure 3.1) consists of four rigid bodies connected to each other by hinges. The contacts between the knife-edged wheels and the flat level surface are modeled by holonomic constraints in the vertical direction, and by non-holonomic constraints in the longitudinal and lateral directions. We assume no-hands operation either with no rider or with a rigid hands-free rider. The resulting non-holonomic mechanical model has three velocity degrees of freedom: forward speed v, lean rate $\dot{\phi}$, and steering rate $\dot{\delta}$.

The following is a brief review of the linearized equations of motion for small perturbations of the upright steady forward motion described in Meijaard *et al.* [6] The linearized dynamics of the lateral and the forward motion are decoupled in this configuration. So, for these linearized equations, the forward speed is constant. The equations of motion for the lateral dynamics are expressed in terms of the rear frame rightward roll angle, ϕ, and the rightward steering angle, δ, both measured relative to the upright straight ahead configuration $[\phi, \delta] = [0, 0]$. At forward speed v the linearized lateral dynamics equations are

$$\mathbf{M}\ddot{\mathbf{q}} + v\mathbf{C}_1\dot{\mathbf{q}} + [g\mathbf{K}_0 + v^2\mathbf{K}_2]\mathbf{q} = \mathbf{f}, \tag{3.1}$$

where the time-varying variables are $\mathbf{q} = [\phi, \delta]^T$ and the generalized torques $\mathbf{f} = [T_\phi, T_\delta]^T$. The first torque, T_ϕ, is an external roll torque on the rear frame, about the ground contact line (more generally, T_ϕ is the work-conjugate of bicycle lean). The second, T_δ, is an internal steering torque acting positively on the front handlebars and negatively on the rear frame (the work conjugate of steer).

We will set the lean and steer torques to zero, but they are left in the equations to help with interpretation. The subscripts for the $\mathbf{C}$ and $\mathbf{K}$ matrices are chosen to match the exponents of the v multipliers.

The constant entries in matrices $\mathbf{M}$, $\mathbf{C}_1$, $\mathbf{K}_0$ and $\mathbf{K}_2$ have the following structure,

$$\mathbf{M} = \begin{bmatrix} M_{\phi\phi} & M_{\phi\delta} \\ M_{\delta\phi} & M_{\delta\delta} \end{bmatrix}, \quad \mathbf{C}_1 = \begin{bmatrix} 0 & C_{1\phi\delta} \\ C_{1\delta\phi} & C_{1\delta\delta} \end{bmatrix},$$
$$\mathbf{K}_0 = \begin{bmatrix} K_{0\phi\phi} & K_{0\phi\delta} \\ K_{0\delta\phi} & K_{0\delta\delta} \end{bmatrix}, \quad \mathbf{K}_2 = \begin{bmatrix} 0 & K_{2\phi\delta} \\ 0 & K_{2\delta\delta} \end{bmatrix}. \tag{3.2}$$

Each of the matrix entries is defined in terms of the 25 design parameters in Meijaard *et al.* [6]

Briefly, $\mathbf{M}$ is a symmetric positive-definite mass matrix which gives the kinetic energy of the bicycle system at zero forward speed by $\dot{\mathbf{q}}^T\mathbf{M}\dot{\mathbf{q}}/2$. The damping-like (there is no real damping) matrix $\mathbf{C} = v\mathbf{C}_1$ is linear in the forward speed v and captures gyroscopic torques due to steer and lean rate, inertial reaction from the rear frame yaw rate (due to trail), and inertial reaction from yaw acceleration proportional to steer rate. The stiffness matrix $\mathbf{K}$ is the sum of two parts: a velocity-independent symmetric part $g\mathbf{K}_0$ proportional to the gravitational acceleration, which can be used to calculate changes in potential energy with $\mathbf{q}^T[g\mathbf{K}_0]\mathbf{q}/2$; and a part $v^2\mathbf{K}_2$ which is quadratic in the forward speed and is due to gyroscopic and centrifugal effects. With these coefficient matrices and the assumption of exponential motions $\mathbf{q} = \mathbf{q}_0 \exp(\lambda_i t)$, the characteristic equation,

$$\det\left(\mathbf{M}\lambda^2 + v\mathbf{C}_1\lambda + g\mathbf{K}_0 + v^2\mathbf{K}_2\right) = 0, \tag{3.3}$$

can be formed and the eigenvalues (roots of the polynomial), λ_i, can be calculated.

Chapter 4

The characteristic polynomial and the Routh stability criteria

The stability of lateral motions of an uncontrolled bicycle is determined by the four eigenvalues calculated from the characteristic equation (3.3). Real roots define exponential behavior, corresponding to exponential growth of lean and steer angles if the roots are positive and to decays of lean and steer angles if the eigenvalues are negative. Complex roots come in complex conjugate pairs and are associated with exponentially growing or decaying oscillatory motion depending on the signs of their real parts.

For common bicycle and motorcycle geometries at low speed there are typically four real roots which transition to two real roots and a complex pair with increasing speed. The smaller (positive or negative) real root is associated with a so-called *capsize* mode where the motion is an ever tightening spiral in which both lean and steer angles slowly increase in proportion. The complex pair is associated with a *weave* mode involving oscillations of both lean and steer; the real part of the weave root can be positive (unstable) or negative (stable). The third remaining eigenmode is called *castering mode* where the steering rapidly aligns with the frame. The castering mode is typically associated with a large negative real eigenvalue (stable). However, for arbitrary bicycles moving at arbitrary speeds the roots are generally not so simply categorized.

For asymptotically stable bicycle motions all eigenvalue real parts must be negative. The characteristic equation for the two degree of freedom lateral motions of the bicycle model (3.3) is a fourth order polynomial in λ, whose roots are the eigenvalues λ_i,

$$A\lambda^4 + B\lambda^3 + C\lambda^2 + D\lambda + E = 0. \tag{4.1}$$

The coefficients of this polynomial are themselves polynomials in the forward speed v:

$$\begin{aligned} A &= A_0 \\ B &= B_1 v \\ C &= C_0 + C_2 v^2 \\ D &= D_1 v + D_3 v^3 \\ E &= E_0 + E_2 v^2. \end{aligned} \tag{4.2}$$

The individual coefficients for v (e.g., $A_0, B_1, \dots$) are lengthy expressions in the 25 bicycle parameters. The Routh [15] stability criteria now state that for all eigenvalues λ satisfying the quartic characteristic equation (4.1) to have a negative real part, all polynomial coefficients A, B, C, D, E and the Routh determinant $X = BCD - ADD - EBB$ must have the same sign. This last determinant is a sixth order polynomial in v of the form,

$$X = X_2 v^2 + X_4 v^4 + X_6 v^6, \tag{4.3}$$

where the coefficients (X_2, X_4 and X_6) are even longer expressions in terms of the 25 bicycle parameters.

The first coefficient $A = A_0 = \det(\mathbf{M}) > 0$ because the mass matrix is positive-definite (except for special singular mass distributions). Thus for stability we need all of B, C, D, E, and X to be positive. For a conventional bicycle design, B_1, C_2, D_3, E_0 are positive and C_0, D_1, E_2 are negative. One simple summary of the entire main paper and of this supplement is the following.

> Because the dependence of these coefficients on the 25 bicycle parameters is complicated there is no simple way to describe what bicycles are stable and at what speeds.

However, for some simple designs such as the theoretical two-mass-skate (TMS) bicycle (see Chapter 7), some general results have been found.

Throughout our discussion of what is and is not possible we assume that no mass is negative, and that all mass is above the ground (i.e., we do not consider bicycles on elevated roads that have mass hanging below the road).

The apparently erroneous conclusion of Klein and Sommerfeld [11] (p. 866) that the gyroscopic action is essential for self-stability is based on their analysis of the D coefficient above. The errors and their implications in the Klein and Sommerfeld analysis are described in Chapter 2 of [3].

The special roles of E and X in the Routh criteria

An uncontrolled bicycle that exhibits stability has all four eigenvalues in the left half of the complex plane. These eigenvalues are either real (representing exponential decay), or complex pairs symmetric about the real axis (representing damped oscillations). As a set there be 4 real eigenvalues, or 2 real and one complex pair, or 2 complex pairs. With continuous change of a parameter (e.g., speed, a mass, or a geometric dimension), these eigenvalues change continuously. Sometimes a complex pair coalesces at the real axis and splits apart as two reals. Or in the opposite case, two real eigenvalues coalesce and split apart as a complex pair.

Stability is lost when any eigenvalue attains a zero real part, then travels further into positive real territory. Generically this can occur in only two ways:

A) A single real eigenvalue takes on the value zero. This is possible only when the E coefficient in the characteristic equation is zero. Near this transition the eigenvalue can be estimated as $\lambda = -E/D$.

B) A pair of complex eigenvalues, symmetric about the horizontal (real) axis, moves to sit on the vertical (imaginary) axis. In other words a purely imaginary eigenvalue pair is a condition of neutral stability. The existence of such a solution to the characteristic equation is expressed by $X = 0$.

The condition for the existence of a pair of purely imaginary roots, $X = 0$, can easily be derived as follows [5]. If we assume that the characteristic equation has one pair of purely imaginary roots then it should have the form

$$(A\lambda^2 + B\lambda + P)(\lambda^2 + Q) = 0. \tag{4.4}$$

Expanding and comparing powers of λ with (4.1) gives us the following three equations for the two unknown coefficients P and Q,

$$AQ + P = C, \quad BQ = D, \quad PQ = E. \tag{4.5}$$

Using the first two equations to solve for P and Q and substitution into the third equation gives us the condition for the existence of one pair of purely imaginary roots

$$\underbrace{BCD - ADD - EBB}_{X} = 0 \qquad \Longrightarrow \qquad X = 0. \tag{4.6}$$

Therefore we have:

> *From a condition of stability (where A, B, C, D, E and X are all positive) X or E will vanish before $B, C,$ or D. Stability is only lost by either E or X passing through zero. Thus all stability boundaries as v is varied are at either $X = 0$ or $E = 0$ (sometimes called the D-decomposition [8]).*

This picture can be more complicated in singular cases in which a parameter variation makes two conditions vanish simultaneously, for example D and X. In that case one boundary is formed by both $D = 0$ and $X = 0$.

Chapter 5

A necessary condition for self-stability: in a steady left turn the torque on the handlebars is to the right

Our interest is *no-hands* riding with no applied steering torque (i.e., zero on the right hand side of Eq. 3.1). But one of the necessary conditions for the self-stability (no-hands stability) of a bicycle, $E > 0$, can be expressed in terms of the *hands-on* control torque needed in one special situation, a steady turn. We derive the result here, and also give some interpretations.

We are interested in the 'handlebar torque' T_δ, the torque applied *to* the handlebars from the rider, needed to hold a steady turn (constant ϕ, constant δ). A clockwise (right) torque on the handlebars ($T_\delta > 0$) causes a clockwise (right) angular acceleration of the steering as long as no gyro torque or other forces are acting on the front assembly.

Start with the linearized equations of motion (3.1). Now consider only steady solutions where there is an applied steer torque T_δ but no applied lean torque. All terms involving $\dot{\mathbf{q}}$ or $\ddot{\mathbf{q}}$ drop out, giving

$$[g\mathbf{K}_0 + v^2\mathbf{K}_2] \begin{bmatrix} \phi \\ \delta \end{bmatrix} = \begin{bmatrix} 0 \\ T_\delta \end{bmatrix}. \tag{5.1}$$

The first line of this equation gives the ratio of lean to steer in all turns at a given v. Using this ration to eliminate ϕ from the second equation we find (using that $K_{0\phi\phi} = m_{\mathrm{T}} z_{\mathrm{T}}$ from Meijaard *et al.* [6]),

$$T_\delta = \frac{\det(g\mathbf{K}_0 + v^2\mathbf{K}_2)}{g m_{\mathrm{T}} z_{\mathrm{T}}}\delta. \tag{5.2}$$

The numerator of (5.2) is the determinant of the total stiffness matrix, which is the constant term E from the characteristic equation (4.1),

$$E = E_0 + E_2 v^2 = \det\left(g\mathbf{K}_0 + v^2\mathbf{K}_2\right). \tag{5.3}$$

Recall that E must be positive for stability. The denominator of (5.2) has gravitational acceleration g, total mass m_{T} and the height z_{T} of the center of mass of the total system (with the positive z-axis pointing down). Thus the denominator is always negative. So:

$$\text{self-stability} \implies E > 0 \implies \mathrm{sgn}(T_\delta) = -\mathrm{sgn}(\delta). \tag{5.4}$$

In words:

> *A necessary condition for a bicycle to have self-stability is that the steady turn torque applied by the rider is of the opposite sign of the handlebar angle.*

Thus, to keep a self-stable bicycle in a rightward (clockwise looking down) circle the rider must apply a leftward (counter-clockwise) torque to the handlebars; in other words, the rider is restraining the handlebars from turning even further.

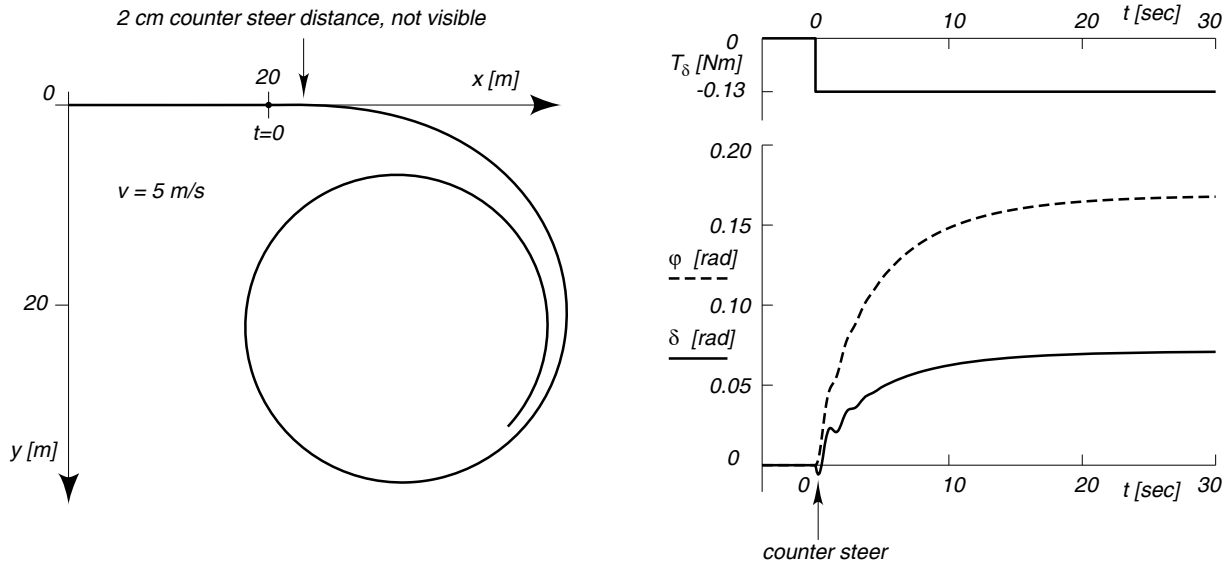

Figure 5.1: Left: front wheel ground track for a bicycle getting into a steady turn. From a state of straight-ahead stable riding at 5 m/s a leftward (CCW, negative) steering torque T_δ is applied as a step function (Right Top). This CCW torque causes a very short small (barely visible as a negative dip in the steer angle curve (Right Bottom)) CCW turn of the handlebars which serves as counter-steering for the subsequent turn into a steady CW (right) turn. Note, $\delta < 0$ is a leftward handlebar turn. The counter-steering is barely visible on the track as it only displaces the track 2 cm to the left before the eventual turn to the right. Note that the applied torque is only about 0.13 Nm (about one poundforce inch).

Counter-steering. For all bicycles initially going straight ahead, a turn to the right is accomplished by counter-steering: rotating the handlebars briefly to the left and then quickly, after the bicycle has fallen somewhat to the right, to the right. For a self-stable bicycle this leftward-then-rightward rotation steer *angle* can all be accomplished by applying a single leftward (counter-clockwise) step in *torque* (with subsequent constant sign and magnitude). The simulations shown are based on the benchmark bicycle [6]. A constant torque of one fixed sign automatically accomplishes the counter-steering, as shown in Figure 5.1. (Note: Of course in a normal riding maneuver a rider does not wait for 12 seconds to attain a desired lean angle. Initially a large torque is applied, leading to a faster roll, and is the reduced to maintain the turn.)

The short time response to a suddenly applied steer torque T_δ is determined by the equation

$$\mathbf{M} \begin{bmatrix} \ddot{\phi} \\ \ddot{\delta} \end{bmatrix} = \begin{bmatrix} 0 \\ T_\delta \end{bmatrix} \tag{5.5}$$

from which we can solve the steer angle acceleration in terms of the steer torque as

$$\ddot{\delta} = \frac{I_{\mathrm{T}xx}}{\det(\mathbf{M})} T_\delta, \tag{5.6}$$

where $I_{\mathrm{T}xx} > 0$ is the mass moment of inertia of the whole bicycle about the forward axis going through the rear contact point P (see Figure 3.1). Because the mass matrix is positive definite we thus have that the first motion after the sudden application of a leftward applied torque is a leftward steer. However, for a self-stable bicycle the long time response, from Eq. 5.4 is a steady right turn (with the left torque still applied)

Similarly, if a self-stable bicycle is in a steady turn to the right, and if the steer torque is suddenly removed, the first motion will be a steer to the right, after which the bicycle will return

to upright straight rolling. It is in this sense that we can make precise the intuitive notion that a self-stable bicycle must turn toward a fall:

> *If steer control is suddenly removed from a state of steady turning, the first motion is to turn more.*

In summary, we have the following mutually equivalent necessary conditions for a bicycle to be self-stable:

1. The characteristic polynomial coefficient $E > 0$.
2. The eigenvalues of the stiffness matrix $\mathbf{K}$ are both negative.
3. $\det(\mathbf{K}) > 0$
4. In a steady circular turn (i.e., constant steer angle and constant lean angle), $\text{sgn}(T_\delta) = -\text{sgn}(\delta)$: the steer torque *opposes* the steer angle (e.g., a steady turn to the right can be accomplished by a forward push on the right handlebar).
5. When control torque of a steady circular turn is released, the first motion is a further turn towards the side of the lean.

Recall that this is only one necessary condition. For stability we also need $B, C, D, X > 0$.

More about the E coefficient: the capsize speed

For self-stability we have the necessary condition that

$$E = E_0 + E_2 v^2 = \det(\mathbf{K}) = \det(g\mathbf{K}_0 + v^2\mathbf{K}_2) > 0. \tag{5.7}$$

For an understanding of 'capsize' (defined below) we would like to consider when this inequality is met or not. For the general Whipple model (Figure 3.1), as described in Meijaard *et al.* [6], E_0 and E_2 are

$$\begin{aligned} E_0 &= -g^2 S_\text{A}(m_\text{T} z_\text{T} \sin\lambda_\text{s} + S_\text{A}), \\ E_2 &= g\cos\lambda_\text{s}(S_\text{F} m_\text{T} z_\text{T} \sin\lambda_\text{s} + (S_\text{F} + S_\text{R})S_\text{A})/w. \end{aligned} \tag{5.8}$$

The terms in (5.8) are the acceleration of gravity g, the total mass m_T, the height of the total mass z_T (negative, with the z-axis down, located at the rear wheel contact), the steer axis tilt λ_s, the front and rear gyrostatic constants $S_\text{F} = I_{\text{F}yy}/r_\text{F}$ and $S_\text{R} = I_{\text{R}yy}/r_\text{R}$, the front and rear wheel mass moments of inertia about the hub axis $I_{\text{F}yy}$ and $I_{\text{R}yy}$, the front and rear wheel radii r_F and r_R, the wheelbase w, a frequently appearing static moment term $S_\text{A} = m_\text{A} u_\text{A} + \mu m_\text{T} x_\text{T}$, with front assembly mass m_A, the perpendicular distance that the center of mass of the front assembly is in front of the steer axis u_A, the horizontal distance of the total mass with respect to the rear contact point x_T, and the dimensionless mechanical trail $\mu = (c/w)\cos\lambda_\text{s}$, where c is the trail.

Interpretation of E_0. At zero speed the stiffness matrix $\mathbf{K}$ is determined solely by the potential energy of the bicycle as a function of lean and steer. In the straight ahead configuration the bicycle cannot be at a potential energy minimum because falling without steering reduces the energy. So at least one of the eigenvalues of $\mathbf{K}_0$ is negative. Thus either

a) $\mathbf{K}_0$ is negative definite and both eigenvalues of $\mathbf{K}_0$ are negative. Then $\det(g\mathbf{K}_0) = g\lambda_1'\lambda_2' = E_0 > 0$. In this case the straight-ahead configuration is a potential energy maximum. Or,

b) $\mathbf{K}_0$ is indefinite and the eigenvalues have opposite sign. Then $\det(g\mathbf{K}_0) = g\lambda_1'\lambda_2' = E_0 < 0$. The potential energy then has a saddle at the straight-ahead configuration and the potential energy can rise for some steer and lean combinations.

For a typical modern bicycle the potential energy is at a local maximum in the upright straight-ahead configuration: every combination of leaning and steering lowers the center of mass. For example, when leaning without steering the whole bike is like an inverted pendulum. And that steering without leaning lowers the system center of mass can be detected by the tendency for the steering to flop to one side or the other when a bicycle is held still and upright. In more detail, for a typical modern bicycle $E_0 > 0$ because $|m_{\mathrm{T}} z_{\mathrm{T}} \sin\lambda_{\mathrm{s}}| \gg S_{\mathrm{A}} > 0$ (and $z_{\mathrm{T}} < 0$). Note that E_0 cannot be positive if the tilt λ_{s} is zero because then $E_0 = -(gS_{\mathrm{A}})^2$. Allowing design changes, the magnitude and sign of E_0 can be adjusted by altering masses, altering geometry, or adding a negative spring to the steering.

Interpretation of E_2. The expression for E_2 has the gyroscopic terms S_{F} and S_{R} as multipliers. A typical modern bicycle has positive and approximately equal gyroscopic terms, $S_{\mathrm{F}} > 0$ and $S_{\mathrm{R}} > 0$, and head angle less than 90° ($\lambda_{\mathrm{s}} > 0$). Keeping in mind that the above relations involving z_{T} and S_{A}, normally $E_2 < 0$ (recall that $z_{\mathrm{T}} < 0$).

Considering a wider variety of conceivable designs, the magnitude and sign of E_2 can be changed/adjusted by the addition of counter-rotating wheels or by adjusting the tilt axis λ_{s}. One way to make E_2 vanish is if there are no gyroscopic contributions from the wheels. Another way to make E_2 vanish is by reducing the steer axis tilt λ_{s} such that

$$\sin\lambda_{\mathrm{s}} = -((S_{\mathrm{F}} + S_{\mathrm{R}})/S_{\mathrm{F}})(S_{\mathrm{A}}/(m_{\mathrm{T}} z_{\mathrm{T}})). \tag{5.9}$$

This is not an explicit formula for the needed steer axis tilt λ_{s} because its cosine is part of S_A. For the benchmark bicycle [6], we find such a zero for E_2 when λ_{s} is close to 2.6 degrees and no other parameters are changed. It turns out if (5.9) is satisfied then $E_0 = g^2 S_{\mathrm{A}}^2 S_{\mathrm{R}}/S_{\mathrm{F}}$ which is necessarily positive if S_{R} and S_{F} are of the same sign.

Capsize speed. As noted above, for a typical modern bicycle $E_0 > 0$ and $E_2 < 0$ so $E = E_0 + E_2 v^2$ changes from positive (allowing the possibility of self-stability, depending on other coefficients) to negative (self-stability is not possible) as speed increases. The transition speed

$$v = \sqrt{-E_0/E_2} \tag{5.10}$$

is called the 'capsize speed'. At this speed the steady turn steer torque vanishes [28] and the characteristic equation (4.1) has one root which is zero. The eigenvector (mode) associated with this zero eigenvalue is a steady turn (constant ϕ, constant δ) of arbitrary radius.

Rice [29] noted the change in sign of quasi-static steer stiffness (i.e., the coefficient of δ in equation (5.2)) namely a 'control reversal' at the onset of the capsize instability, and called the critical speed or the "inversion speed".

Because both E_0 and E_2 can have either sign or be zero, there are a number of ways to meet the necessary stability condition $E = E_0 + E_2 v^2 > 0$. These are shown in Figure 5.2 below or by the following enumeration.

$E_0 > 0, E_2 < 0$. This is the common situation for modern bicycles: self-stability is only possible at speeds v below the capsize speed.

$E_0 < 0, E_2 < 0$. The potential energy has a saddle, and both the gyro (spin angular momentum) terms and the head angle have their common values: self-stability is impossible.

$E_0 > 0, E_2 > 0$. The potential energy has a local maximum (the usual situation) and the combination of gyro terms and head angle are negated: self-stability is possible (according to this one Routh criteria) at all speeds. If the bicycle is stable for some speed, the loss of stability as speed increases due to E changing sign does not occur. The bicycle might keep its stability to infinite speed (depending on whether the other critical Routh parameter X changes sign).

$E_0 < 0, E_2 > 0$. The potential energy has a saddle and the combination of gyroscopic terms and head angle are reversed: self-stability is only possible at speeds v above the capsize speed.

In situations where the equation $E_0 + E_2 v^2$ has no real root v, there is no capsize speed. This occurs if E_0 and E_2 have the same sign or if $E_2 = 0$. Thus, for example, setting $E_2 = 0$ eliminates the capsize transition. E_2 can be set to zero various ways, for example by eliminating gyro terms (as in the bicycle in this paper), or by geometric changes.

Note that here we are only considering one of the 5 non-trivial Routh conditions for stability. Even with $E > 0$ satisfied there are many ways a bicycle can be unstable. A figure somewhat analogous to Figure 5.2 but that takes account of all the Routh criteria for the theoretical TMS bicycle highlighted in this paper, is Figure 7.3 on page 34.

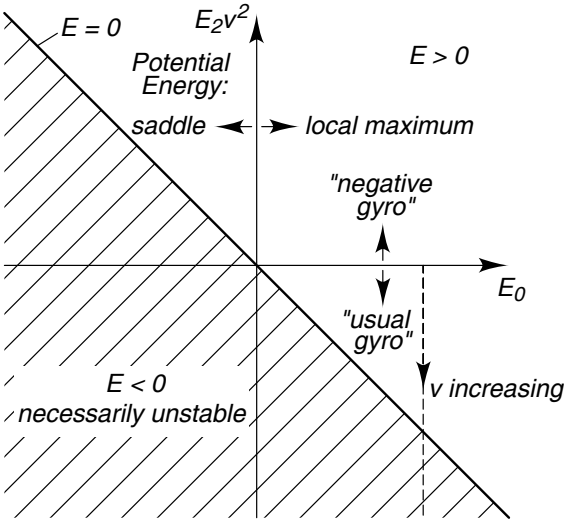

Figure 5.2: Regions where stability is possible ($E > 0$) are unshaded. In the shaded regions stability is impossible. The sign of the E_0 term is determined by the mass distribution and the geometric lay-out. For the right hand plane the potential energy has a local maximum ($E_0 > 0$). The sign of the E_2 "gyro" term is mostly determined by the spin angular momentum of the wheels but is also affected by other parameters, notably the head angle λ_s. For the lower half plane the E_2 "gyro" term is negative. Common bicycles are often in the lower right quadrant with $E > 0$ and $E_2 < 0$. For a given bicycle, increasing the speed v moves E away from the x-axis. For the case $E_0 > 0$ and $E_2 < 0$ this is shown by the dashed line 'v increasing' in the lower right quadrant. Crossing the $E = 0$ line occurs at the capsize speed. Thus there is no capsize speed in the upper right quadrant. In the upper left quadrant an upwards v increasing line could be constructed, indicating that stability would be possible at sufficiently great speeds. The dependence of E_0 and E_2 on parameters is discussed in more detail with regard to the theoretical two-mass-skate (TMS) bicycle in Chapter 7.

Chapter 6

Counterexamples: bicycles which are self-stable or not, despite common lore

There are various ways in which stability can be gained or lost by adjusting one or more of the 25 bicycle parameters in the Whipple bicycle model [6]. In this chapter a number of examples are given which show that no combination of positive (i.e., forward spinning) gyroscopic action, or positive trail, or positive steer axis tilt, are either necessary, or sufficient for self-stability over at least a small range of speeds. The examples are calculated with the help of JBike6 [30], a Matlab program for performing the bicycle eigenvalue calculation. The usage and output of JBike6 is explained below.

The nine cases below, seven of which are detailed on the following pages, give the flavor of the situation.

A) **Benchmark bicycle.** The benchmark bicycle from Meijaard *et al.* [6] is not presented again here. That bicycle is similar to bicycles of common construction including an attached rigid no-hands rider. It has spin angular momentum in the wheels (gyros) and positive trail. It has a self-stable speed range from about 4.3 m/s to 6 m/s. By 'benchmark bicycle' we mean not just the model in Meijaard *et al.* but exactly the particular high-precision parameter values given in the main example in Meijaard *et al.*

B) **Self-stable with no gyro and negative trail.** A bicycle that has negative trail and zero gyro yet is self-stable. This two-mass-skate (TMS) bicycle is the main topic of the paper. It is presented in the main text and is described in detail in Chapter 7. It is not repeated here.

1) **Benchmark bicycle, unstable with no gyro.** The benchmark bicycle entirely loses its stability if it is only changed by the removal of the wheel gyro terms, confirming the narrowest interpretation of the conclusion of K&S. This is the first of several examples below based on making small changes to the benchmark bicycle from Meijaard *et al.* [6]

2) **Benchmark bicycle, unstable with negative trail.** The benchmark bicycle entirely loses its stability if the trail is made negative by displacing the steer axis rearward while leaving the wheel position and mass locations unchanged. K&S were concerned with gyros, not trail, so missed that trail is just as important.

3) **Benchmark bicycle, with gyro and positive trail but unstable if the mass distribution is changed.** A bicycle that is conventional in that it has positive trail and positive gyro but is unstable at any speed. One might think that trail and wheel spin angular momentum are sufficient for self-stability. They are not.

4) **Stable with negative trail.** Two bicycles based on the benchmark, that are thus more conventional than the TMS bicycle in the main paper, but have negative trail and yet are still

self-stable at some speeds. This example differs from (2) in that the mass distribution was also changed. This provides another proof that positive trail is not necessary for self-stability.

5) **Stable with negative gyro.** A bicycle that is self-stable with negative gyro. This provides another proof that wheel spin angular momentum is not necessary for self-stability.

6) **Stable with steer axis tilt reversed.** A bicycle that is self-stable with a steer axis tilted the reverse of conventional (and also a negative gyro). This proves that the steer axis does not have to have the conventional (rearward) tilt to achieve self-stability.

7) **Stable with rear-wheel steering.** A rear-steered bicycle with vertical steer axis that is self-stable. This proves that rear-wheel steering is not necessarily unstable. It also proves, violating simpler examples from the literature, that self-stability is possible with a vertical steering axis.

How to read JBike6 input. A JBike6 [30] Matlab screenshot is shown in Figure 6.3. First we explain how to read this screen. In the top half the 25 parameters for a bicycle design are specified. Basically four bodies have to be specified: the rear frame, the front frame and the two wheels. The interface allows separate descriptions for the rider and the rear rack but combines these with the rear frame into one rigid body. Likewise the front fork and the front basket are combined into one rigid body. The wheels are assumed to be axisymmetric so only two mass moments of inertia need be specified. The other bodies are assumed symmetric about the vertical plane and the mass moments of inertia are specified by the three principal values and the angle α of the 1-axis with the x-axis in the xy-plane. The program output is in the bottom half of the screen: on the left is a sketch of the bicycle to scale, and on the right is a plot of the eigenvalues as a function of the forward speed. In the bicycle sketch the mass moment of inertia of the wheel is indicated by a radius of gyration circle (concentric with and inside the outer wheel circle). The mass moments of inertia for the other rigid bodies are depicted by 6-mass balls lined up in pairs in the three principal directions. The mass of every ball is 1/6 of the total mass (the circle at the center represents both a right mass and a left mass hidden behind it). The relative volumes (diameter cubed of the circles in the front and rear dumbbells) indicate the relative masses of those two assemblies.

How to read JBike6 output. The eigenvalue plot on the right shows the real (dark dots) and imaginary (light dots) parts of the eigenvalues in the specified forward speed range. Note that the appearance of two light curves (imaginary components symmetrically positive and negative) occurs at the speed where two dark curves coalesce. The coalesced dark curve then represents the real part of the complex pair, and must be negative for stability (in this figure it is positive). The stable speed range, if it exists, is where all (usually 'all' = 'two reals and one real part of a complex pair') dotted dark lines are below zero, and is marked with a thick horizontal bar on the bottom edge of the graph. This is often between the weave and capsize speeds (see Figure 6.4). The weave and capsize speeds, as well as any other boundaries of the stable speed range, are shown as vertical lines (see Figure 6.4). Note that in the benchmark bicycle the front and rear wheels have different sizes. This size difference is for benchmarking purposes and is not significant for the self-stability of a bicycle.

JBike6 versus benchmark coordinates. The JBike6 program uses another coordinate system than the benchmark bicycle paper [6]. In JBike6 the x-axis is forward, the y-axis is up, and the z-axis is to the right (looking forward). In the bicycle benchmark paper the SAE J670 [31] z-down convention is used, with the x-axis forward, the z-axis down, and the y-axis to the right (looking forward). Thus $[x, y, z]_{\text{Benchmark}} = [x, z, -y]_{\text{JBike6}}$. In matrix form the transformation from

the JBike6 coordinate system, denoted by the superscript J, to the benchmark bicycle coordinate system, denoted by superscript B, is

$$\begin{pmatrix} x \\ y \\ z \end{pmatrix}^{\mathrm{B}} = \begin{pmatrix} 1 & 0 & 0 \\ 0 & 0 & 1 \\ 0 & -1 & 0 \end{pmatrix} \begin{pmatrix} x \\ y \\ z \end{pmatrix}^{\mathrm{J}}, \quad \mathbf{x}^{\mathrm{B}} = \mathbf{T}\mathbf{x}^{\mathrm{J}}, \quad \rightarrow \quad \mathbf{x}^{\mathrm{J}} = \mathbf{T}^{T}\mathbf{x}^{\mathrm{B}}. \tag{6.1}$$

The mass moments of inertia matrices transform according to a second order tensor and are $\mathbf{I}^{\mathrm{J}} = \mathbf{T}^{T}\mathbf{I}^{\mathrm{B}}\mathbf{T}$ and $\mathbf{I}^{\mathrm{B}} = \mathbf{T}\mathbf{I}^{\mathrm{J}}\mathbf{T}^{T}$, or written out in components

$$I^{\mathrm{J}}_{xx} = I^{\mathrm{B}}_{xx}, \quad I^{\mathrm{J}}_{xy} = -I^{\mathrm{B}}_{xz}, \quad I^{\mathrm{J}}_{xz} = I^{\mathrm{B}}_{xy}, \quad I^{\mathrm{J}}_{yy} = I^{\mathrm{B}}_{zz}, \quad I^{\mathrm{J}}_{yz} = -I^{\mathrm{B}}_{yz}, \quad I^{\mathrm{J}}_{zz} = I^{\mathrm{B}}_{yy}. \tag{6.2}$$

Finally, in the JBike6 interface, the mass moments of inertia are specified by the three principal values (I_{11}, I_{22}, I_{zz}) and the counterclockwise angle α of the 1-axis relative to the x-axis in the xy-plane, which can be calculated from

$$I_{11,22} = \frac{I_{xx} + I_{yy}}{2} \pm \sqrt{I_{xy}^2 + \left(\frac{I_{xx} - I_{yy}}{2}\right)^2}, \quad \text{and} \quad \alpha = \frac{1}{2}\arctan\left(\frac{2I_{xy}}{I_{xx} - I_{yy}}\right). \tag{6.3}$$

6.1 The benchmark bicycle has no stable region when the gyro is removed

The benchmark bicycle of Meijaard *et al.* [6] has a self-stable speed range. This is the first of 3 examples based on this benchmark. In this first example we just eliminate the gyroscopic term by setting the I_{zz} of the wheels to zero. This calculation is identical in spirit to that done by K&S [11] in which they eliminated the gyro terms from the parameters given by Whipple. As discussed in [3] we agree that a bike with Whipple's parameters loses its stability if the gyro term is removed. As for the bicycle with the Whipple parameters, the benchmark bicycle also loses its stability if the gyro terms are removed.

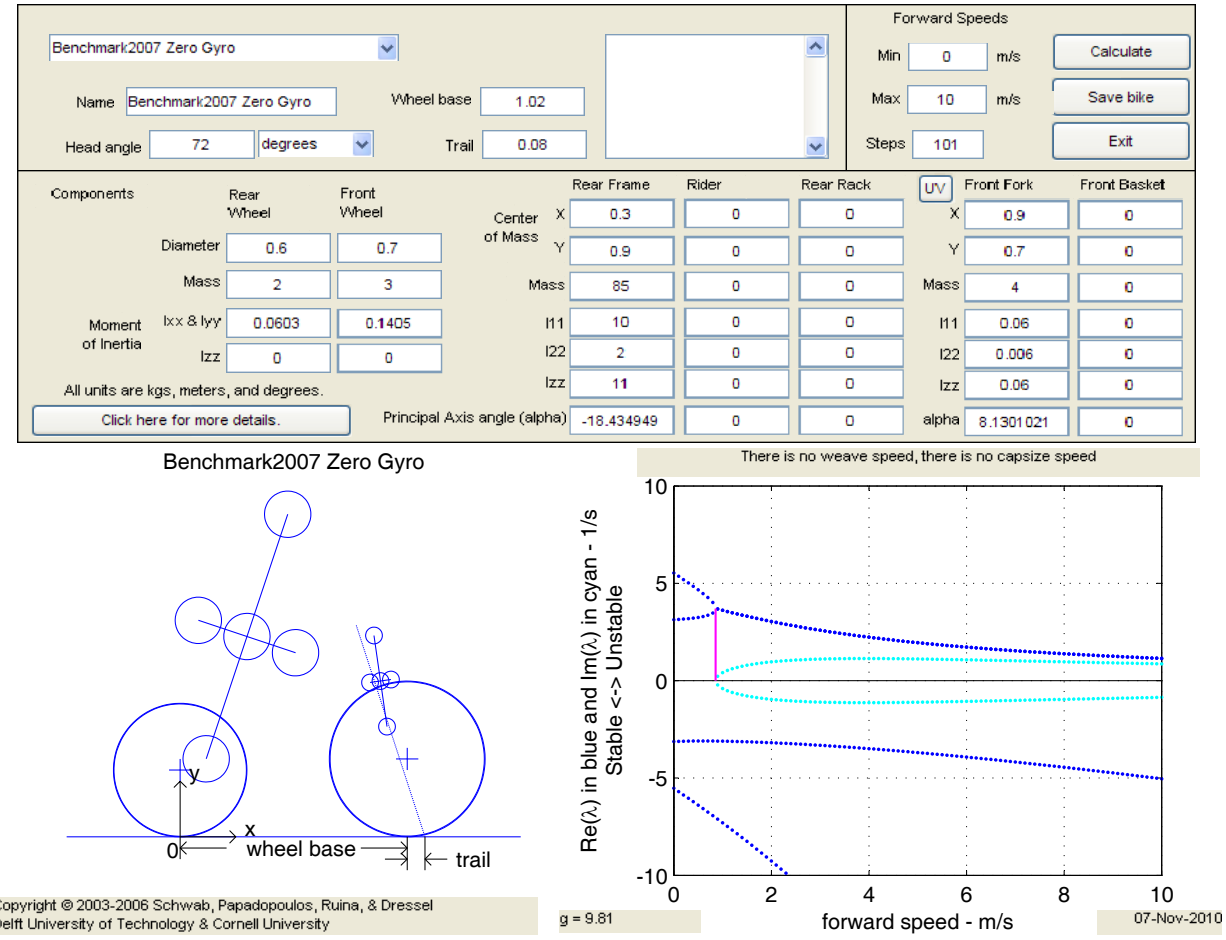

Figure 6.1: A bicycle of common construction but with the gyroscopic terms eliminated. The model is based on the benchmark bicycle [6] where the only change that has been made is to eliminate the spin angular momentum of the wheels. This bicycle is unstable at all forward speeds.

6.2 The benchmark bicycle has no stable region when the trail is made negative

In the spirit of the previous example where the stability of the benchmark bicycle was lost by removing the gyro term, we now manipulate the trail. By making the trail negative (setting the Trail box to -0.009, effectively, this translates the steering axis while leaving all other mass positions and wheels centers unchanged) we lose all self-stability. (Note that when starting with Whipple's own example parameters instead of the benchmark values, stability is also lost when the trail is set to zero.)

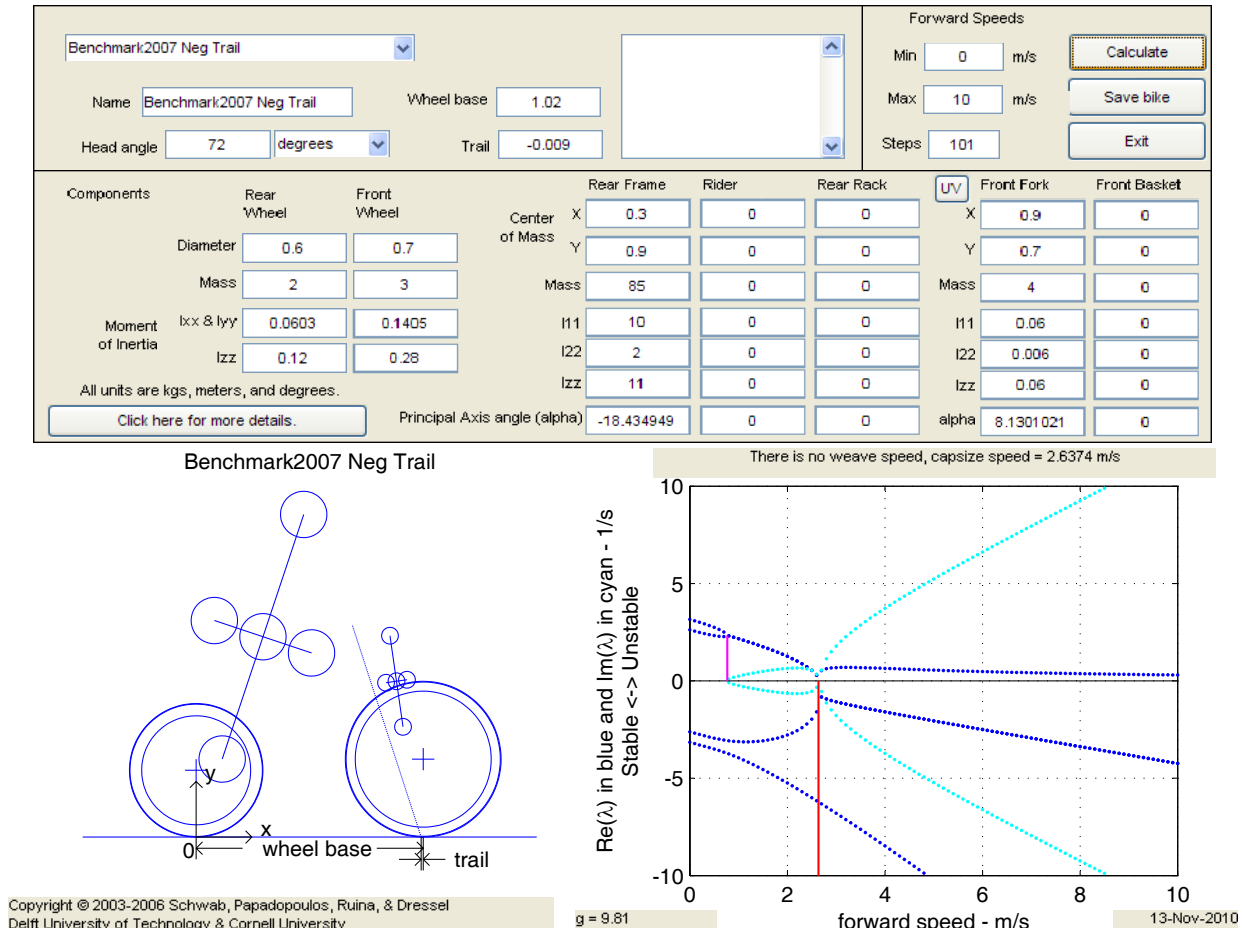

Figure 6.2: A bicycle of common construction but with the trail altered. The model is based on the benchmark bicycle [6] where the only change that has been made is making the trail negative by displacing the steer axis backwards. The self-stability speed range vanishes.

6.3 Lacks any stable speed range even with positive trail and positive gyro

Common bicycles have positive trail and positive gyro terms (the wheels spin clockwise as a bicycle moves from left to right in front of you). Here we demonstrate that these two terms are not sufficient to give self-stability. Our example is based on perturbing the benchmark bicycle [6] by only changing the x-coordinate of the front fork center of mass from 0.9 m to 0.7 m. The result is a bicycle that is not self-stable at *any* speed.

The previous two examples show that the gyro term and trail are necessary to achieve stability of the benchmark bicycle. Here we show that they are not sufficient to guarantee stability.

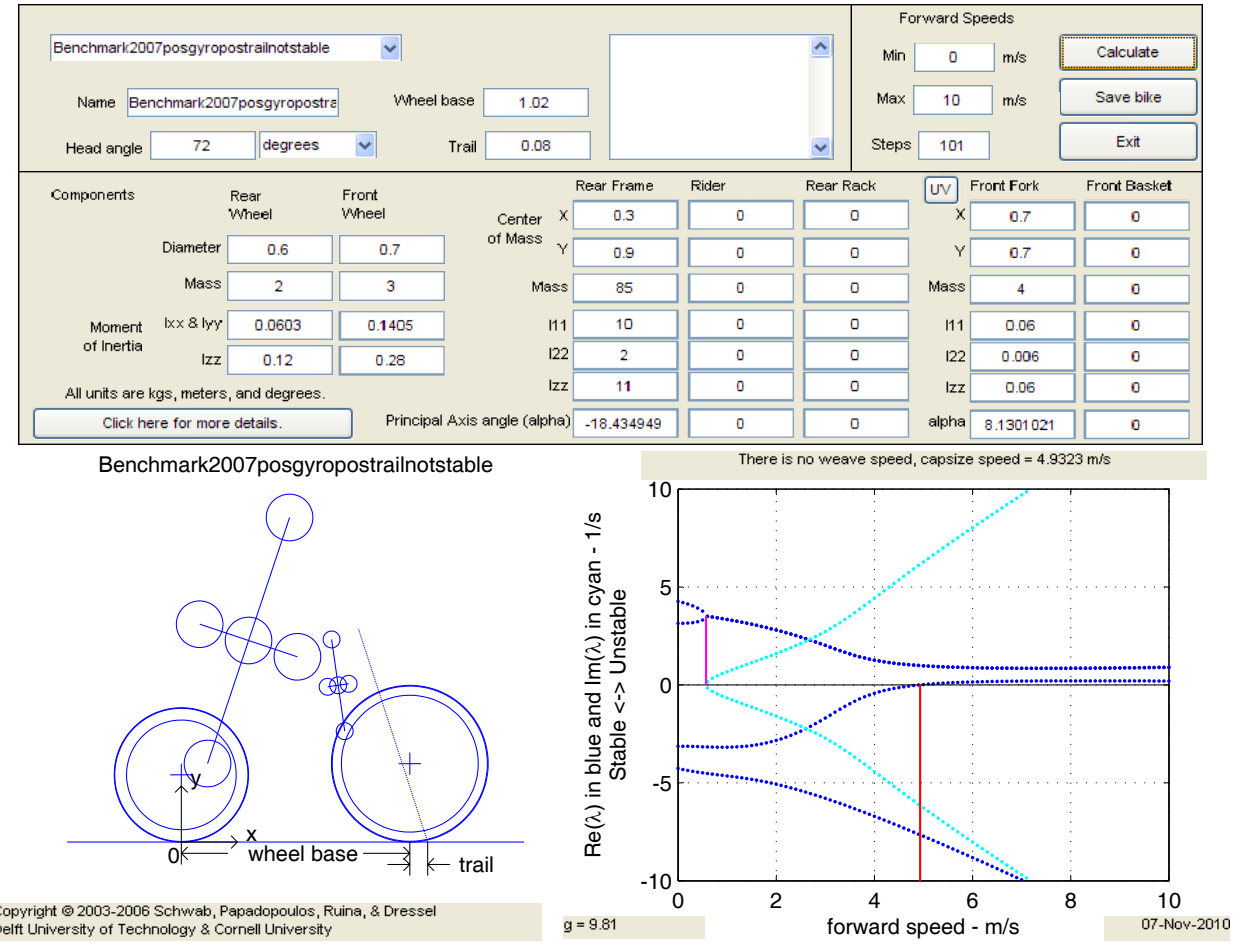

Figure 6.3: A bicycle of common construction with gyroscopic action and positive trail but with no stable forward speed range. The model is based on the benchmark bicycle [6] where the only change that has been made is to place the center of mass of the front fork behind the steer axis instead of in front of it. Clearly the bicycle is unstable at all forward speeds.

6.4 Conventional bicycle displaying stability even with negative trail

While the main paper shows a bicycle with negative trail that has self-stability, that bicycle may be viewed as rather unconventional. The bicycles below have more conventional geometry and mass distribution but have negative trail while maintaining self-stability for some range of speeds. This first example is based on increasing front fork mass but not moment of inertia, and increasing the steer axis tilt.

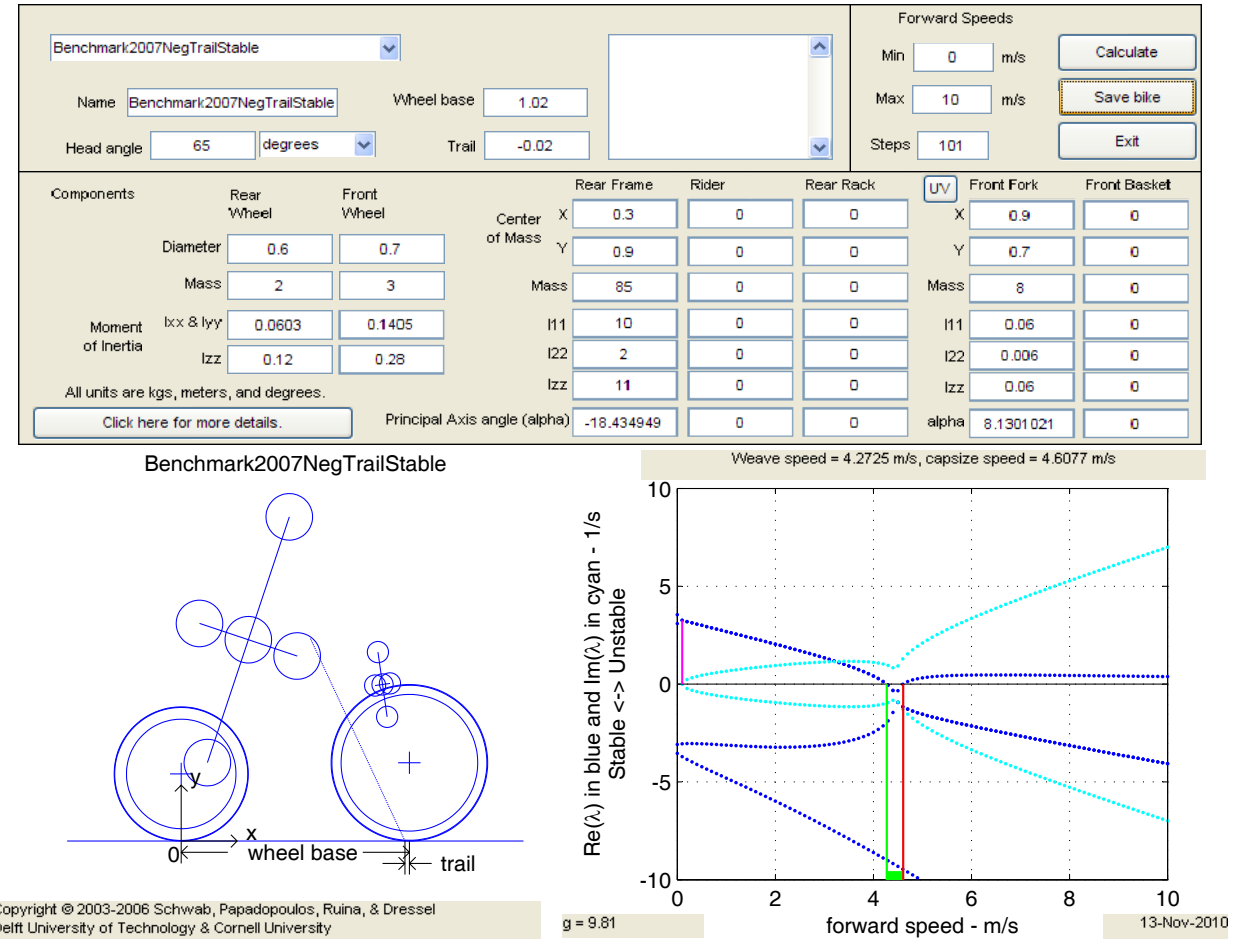

Figure 6.4: A bicycle of common construction but with negative trail, which still shows a stable forward speed range. The model is based on the benchmark bicycle [6] but now with a negative trail of -0.02 m, an increased steer axis tilt of 25 ($= 90 - 65$) degrees and therefore with the center of mass of the front assembly more forward of the steer axis. The front frame mass was also increased. This bicycle still shows a (small) stable forward speed range (between the vertical lines marking the weave and capsize speeds).

Next we present a second example, also based on the benchmark bicycle, and stable with negative trail. In this case the compensating change was the addition of a decentering spring implemented as a control torque $T_\delta = -k\delta$, with $k = -10$ Nm/rad. Physically such a decentering spring can be implemented as a tensile spring from the seat post to a point on the handlebars forward of the steer axis (thus making a toggle-like mechanism). A physical bicycle with negative trail and such a negative spring was demonstrated by Hand [32]. We do not view this as a control system compensating for passive instability, but rather as a change in the passive components that allows negative trail.

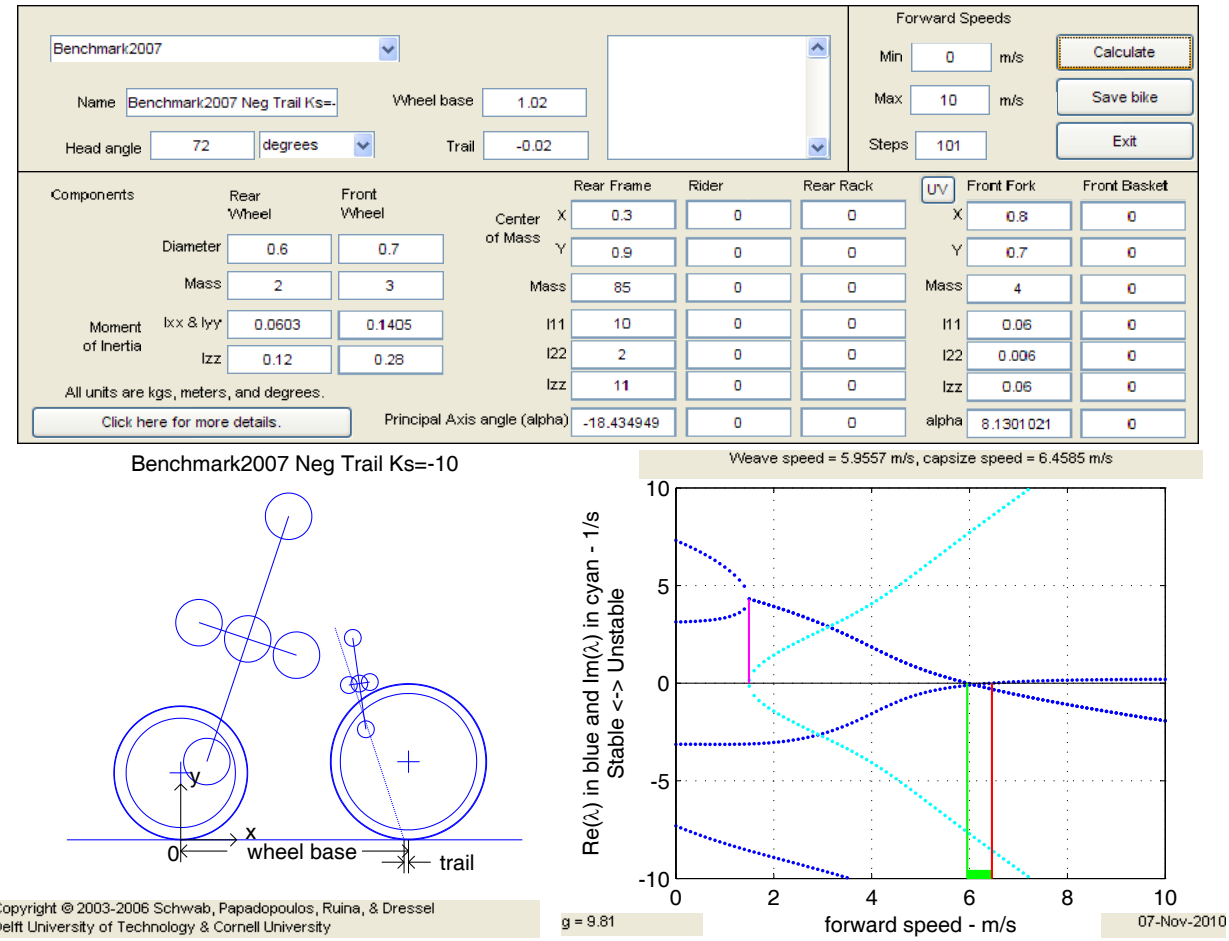

Figure 6.5: A bicycle of common construction but with negative trail, which still shows a stable forward speed range. The model is based on the benchmark bicycle [6] but now with a negative trail and a decentering steering spring ($T_\delta = -k\delta$, with $k = -10$ Nm/rad). This bicycle still shows a (small) stable forward speed range (between the vertical lines marking the weave and capsize speeds).

6.5 Stable with negative gyro

The bicycle described in the main paper had an approximately zero gyro term (exactly zero in theory, approximately zero in physical construction). Here we show that stability is not lost even if there is a slightly negative gyro term for both wheels (e.g., with the counter-rotating wheels more massive than the rolling wheels). The JBike6 wheel polar inertia, I_{zz}, is really the spin angular momentum per unit forward velocity. So a negative polar inertia means that an added counter-spinning wheel, geared to the rolling wheel, has greater spin angular momentum than the regular rolling wheel. For this bicycle the Routh coefficients are such that $E_0 < 0$ (meaning that the potential energy is indefinite) and $E_2 > 0$, the reverse of the situation with a conventional bicycle (in which $E_0 > 0$ and $E_2 < 0$).

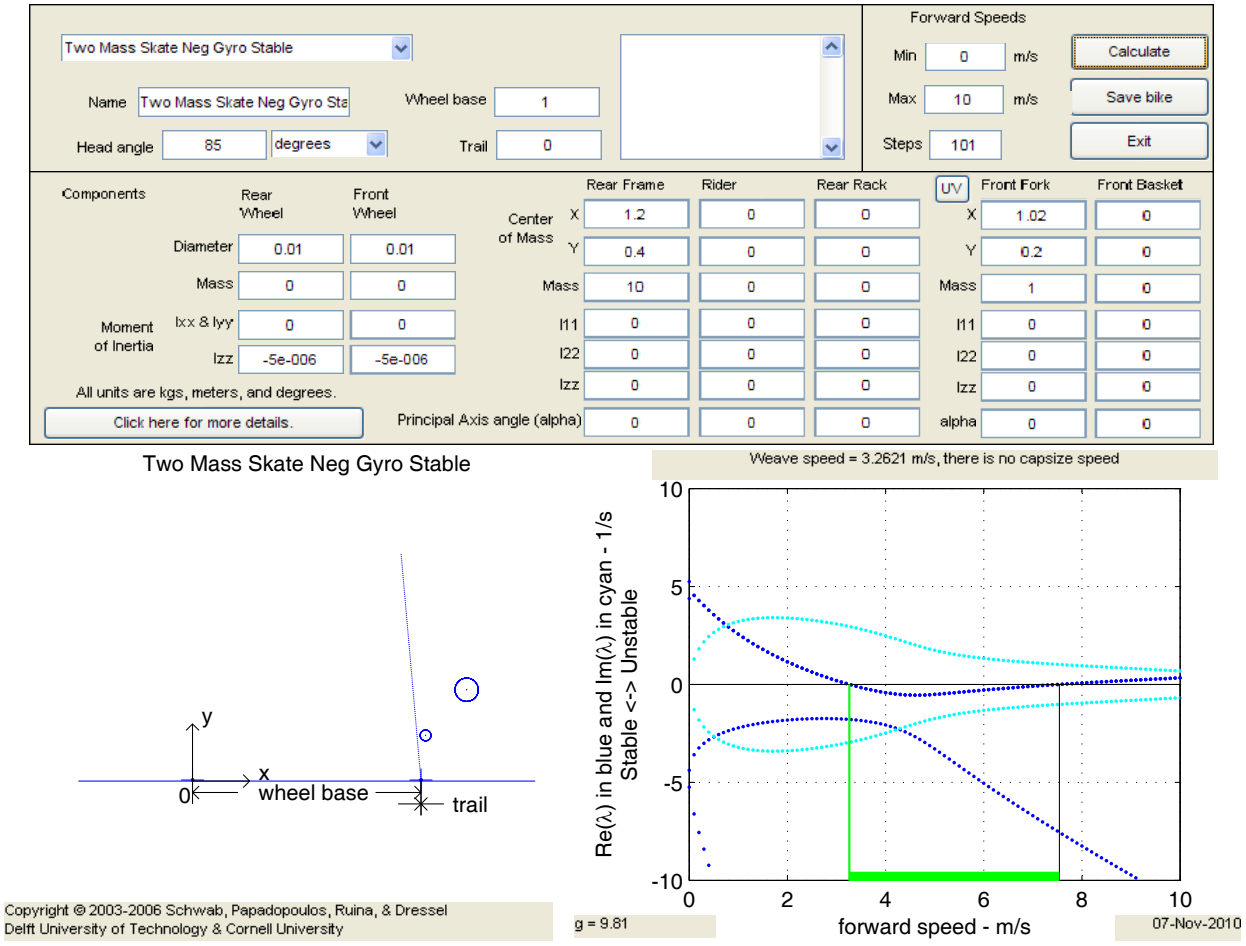

Figure 6.6: The model is based on the theoretical two-mass-skate (TMS) model from Chapter 7, but with slightly negative gyroscopic action (e.g., by counter-spinning wheels) and where the center of mass of the front fork has been lowered to 0.2 m. This bicycle has a large stable forward speed range.

6.6 Stable speed range with a reverse tilted steer axis

In addition to the conventional wisdom about the need for positive trail and positive gyroscopic terms, there is also a conventional wisdom that the head tube of a bicycle must be tipped back (i.e., that we need $\lambda_s > 0$). Here we show a bicycle with steer axis tipped forward, $\lambda_s < 0$ (Head angle = $95°$). This shows as the line leaning $5°$ forward in the lower-left portion of the figure. The example after this one (on rear-wheel steering) demonstrates self-stability when the steering axis is vertical.

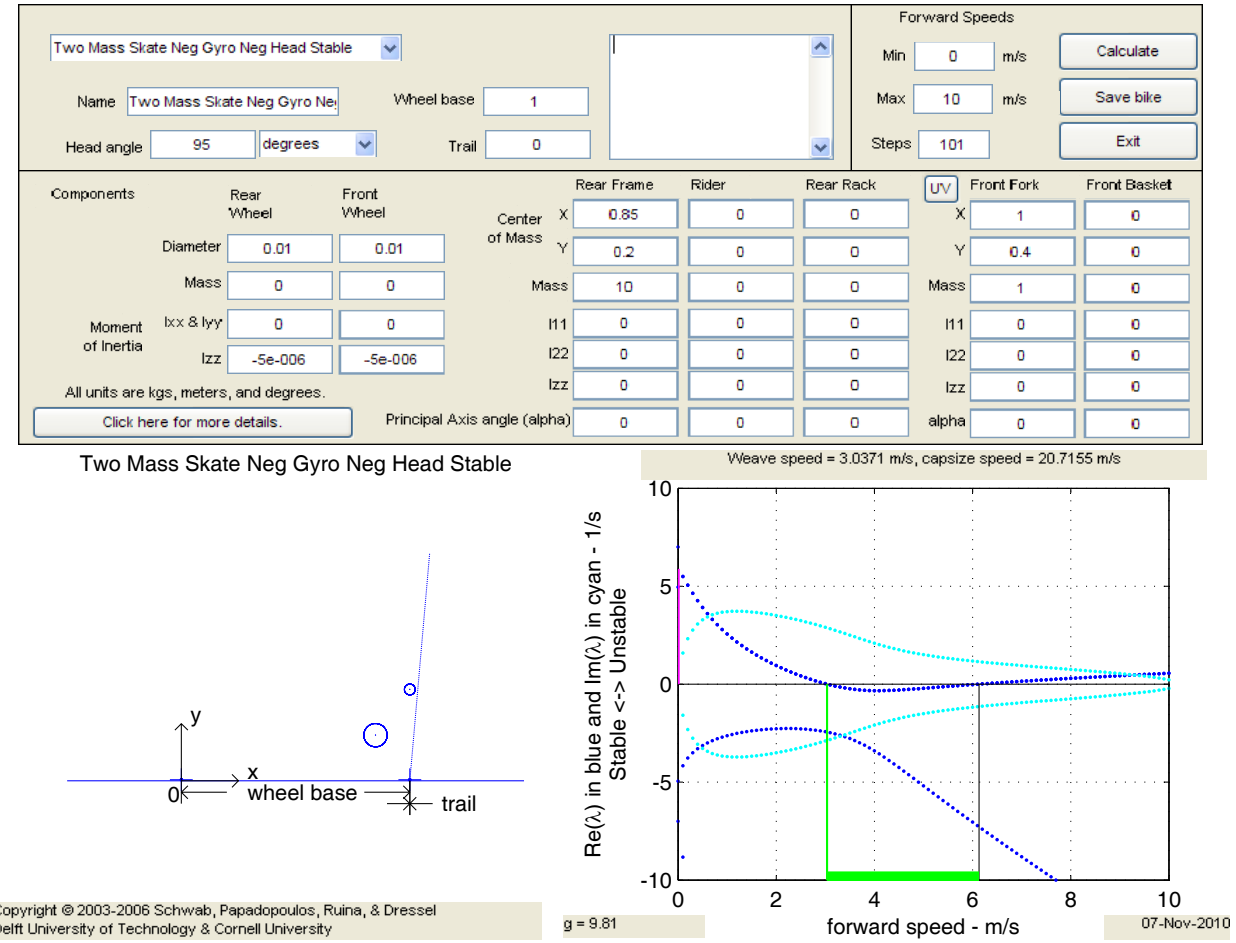

Figure 6.7: A two-mass-skate (TMS) bicycle with negative gyroscopic action, reverse tilted steer axis, which shows a stable forward speed range. The model is based on the alternative theoretical two-mass-skate (TMS) model from Chapter 7, which has a reverse tilted steer axis with added negative gyroscopic action. This bicycle clearly shows a stable forward speed range.

6.7 Stable with rear wheel steering

Another common thought is that a rear-wheel steered bicycle cannot be self-stable, for example that a large positive eigenvalue "is inherent in the rear steered configuration" [33]. Note that the definition of rear-wheeled steering is somewhat problematic because it lacks an objective definition. The Whipple bicycle has a symmetric definition: there is a rear frame connected to a wheel and there is a front frame connected to a different wheel. And the two frames are connected by a hinge. Steering is the control of that hinge angle. If we imagine a sequence of bicycles where more and more mass is put on the front assembly and where the hinge location is put closer and closer to the rear wheel, at what point is the bicycle declared to be 'rear-wheel steering'? With regard to rear-wheel steering, most people think they'd know it if they saw it [34] because for most vehicles the hinge is *much* closer to one wheel than the other and that wheel assembly has *much* smaller mass. Our 'rear-wheel' steering example is of that nature, not objectively rear-wheel steering, but rear-wheel steering just as much as conventional bicycles have front wheel steering.

This example also has a vertical head-tube (shown just forward of the steering rear wheel). By this and the previous example we falsify the plausible conjectures that the steering axis tilt λ_s must be positive or at least non-zero.

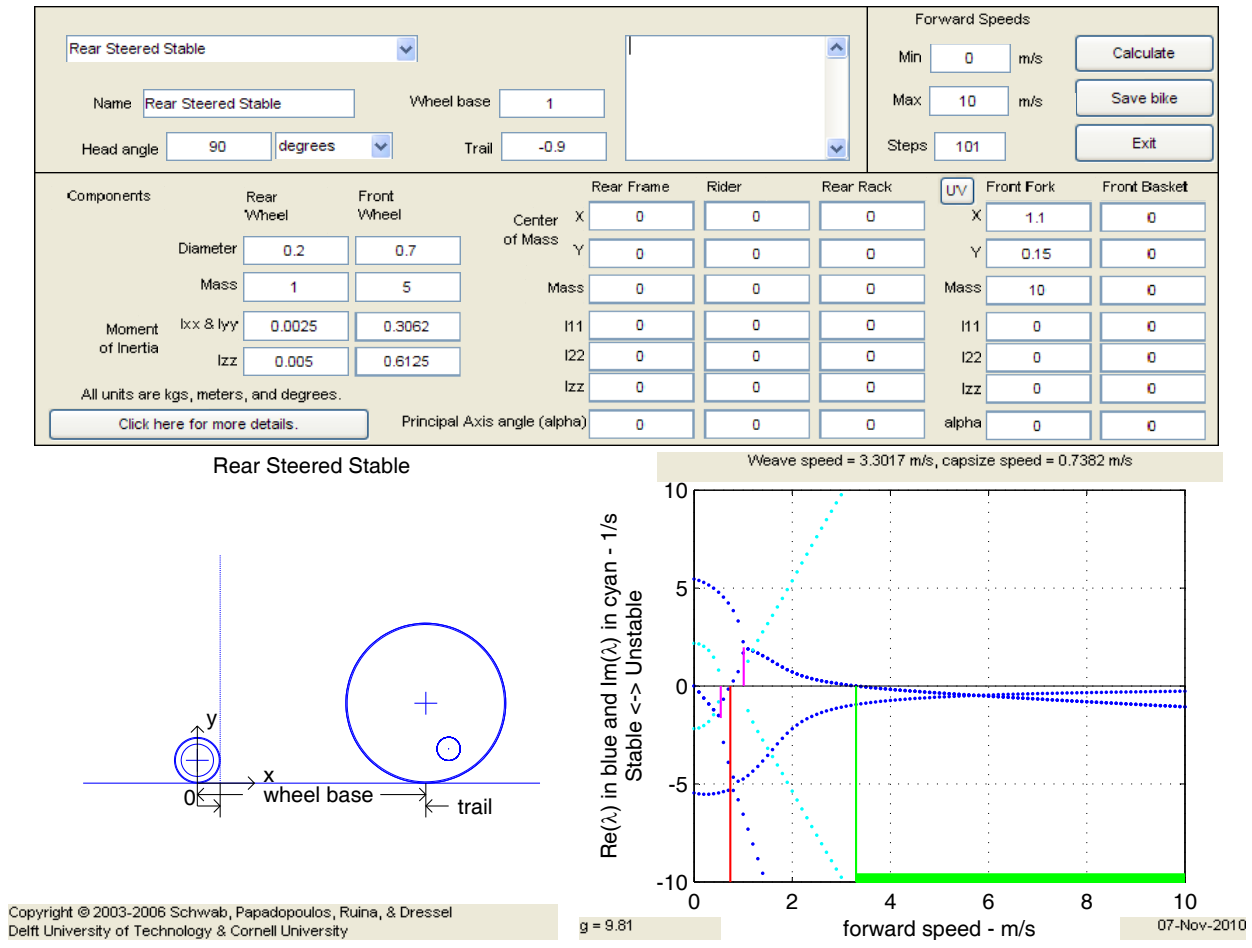

Figure 6.8: A bicycle with 'rear wheel steering' which shows a stable forward speed range. The steer axis is just in front of the rear wheel and is vertical. The heavy front assembly has a center of mass in front of the front wheel. This rear wheel steered design has a stable forward speed range to the right of the rightmost vertical line, from 3 m/s $\rightarrow \infty$.

Part II

DESIGN AND TESTING OF EXPERIMENTAL BICYCLE

Chapter 7

Theoretical two-mass-skate (TMS) bicycle

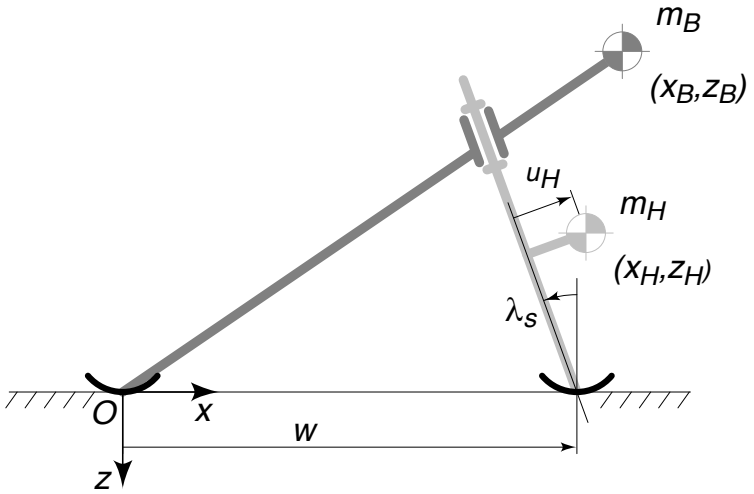

Figure 7.1: Theoretical two-mass-skate (TMS) bicycle. The wheels are replaced with skates.

The complexity of the full 25-parameter Whipple bicycle model (see Chapter 3) makes it hard to probe for theoretical insights. We have focused our investigations on a simplified, or so-called theoretical 'two-mass-skate' (TMS) bicycle introduced in Hand [32] and described in various informal writings of Papadopoulos [14]. The theoretical two-mass-skate (TMS) bicycle has zero trail. It has massless wheels so its dynamics are equivalent to that of a bicycle with ice skates instead of wheels, see Figure 7.1. The mass distribution of the rear and the front frame are those of two point masses. An extra point mass can be added exactly at either contact point with no effect on the lateral balance equations. In our experimental machine, such a mass near the rear contact was used to keep the bicycle from tipping over forward. The theoretical two-mass-skate (TMS) bicycle has only 8 non-zero parameters. These are shown in Figure 7.1 and Table 7.1.

For the full Whipple model, entries in the mass, damping and stiffness matrices ($\mathbf{M}, \mathbf{C_1}$, $\mathbf{K_0}$ and $\mathbf{K_2}$ in Eq. (3.1)) are large expressions. For the theoretical two-mass-skate (TMS) bicycle these matrices are more manageable, taking the form

$$\mathbf{M} = \begin{bmatrix} m_\mathrm{B}\, {z_\mathrm{B}}^2 + m_\mathrm{H}\, {z_\mathrm{H}}^2 & -m_\mathrm{H}\, u_\mathrm{H}\, z_\mathrm{H} \\ -m_\mathrm{H}\, u_\mathrm{H}\, z_\mathrm{H} & m_\mathrm{H}\, {u_\mathrm{H}}^2 \end{bmatrix}, \tag{7.1}$$

$$\mathbf{C}_1 = \begin{bmatrix} 0 & -(m_\mathrm{B}\, x_\mathrm{B}\, z_\mathrm{B} + m_\mathrm{H}\, x_\mathrm{H}\, z_\mathrm{H})/\bar{w} \\ 0 & (m_\mathrm{H}\, u_\mathrm{H}\, x_\mathrm{H})/\bar{w} \end{bmatrix}, \tag{7.2}$$

$$\mathbf{K}_0 = \begin{bmatrix} m_\mathrm{B}\, z_\mathrm{B} + m_\mathrm{H}\, z_\mathrm{H} & -m_\mathrm{H}\, u_\mathrm{H} \\ -m_\mathrm{H}\, u_\mathrm{H} & -m_\mathrm{H}\, u_\mathrm{H}\, \sin\lambda_\mathrm{s} \end{bmatrix}, \tag{7.3}$$

Parameter	**Symbol**	**Value**
Wheel base	w	1 m
Steer axis tilt	λ_s	5°
Rear frame assembly B mass	m_B	10 kg
Rear frame assembly B center of mass	(x_B, z_B)	$(1.2, -0.4)$ m
Front fork and handlebar assembly H mass	m_H	1 kg
Front fork and handlebar assembly H center of mass	(x_H, z_H)	$(1.02, -0.2)$ m

Table 7.1: Parameters and values for a theoretical two-mass-skate (TMS) bicycle. Only non-zero values are mentioned. The values given are for the ideal target-design of the experiments described in Chapters 8–11.

$$\mathbf{K}_2 = \begin{bmatrix} 0 & -(m_B\, z_B + m_H\, z_H)/\bar{w} \\ 0 & (m_H\, u_H)/\bar{w} \end{bmatrix}, \tag{7.4}$$

where we have introduced new redundant parameters to represent two recurring expressions, the distance $u_H = (x_H - w)\cos\lambda_s - z_H \sin\lambda_s$ of the front mass m_H in front of the steer axis, and a projected wheelbase $\bar{w} = w/\cos\lambda_s$. Note that the positive z-axis points down from ground level, so that z-coordinates are all negative. Then the polynomial coefficients of (4.2) and (4.3) from the characteristic equation become:

$$\begin{aligned}
A_0 &= m_B\, m_H\, {u_H}^2\, {z_B}^2 \\
B_1 &= -m_B\, m_H\, u_H\, z_B\, (x_B\, z_H - x_H\, z_B)/\bar{w} \\
C_0 &= -g\, m_H\, u_H \left(m_B \sin\lambda_s\, {z_B}^2 - m_B\, u_H\, z_B + m_H \sin\lambda_s\, {z_H}^2 + m_H\, u_H\, z_H\right) \\
C_2 &= m_B\, m_H\, u_H\, z_B\, (z_B - z_H)/\bar{w} \\
D_1 &= -g\, m_B\, m_H\, u_H\, z_B\, (x_B - x_H)/\bar{w} \\
D_3 &= 0 \\
E_0 &= -g^2\, m_H\, u_H\, (m_H\, (x_H - w)\cos\lambda_s + m_B\, z_B \sin\lambda_s) \\
E_2 &= 0 \\
X_2 &= -g^2\, ({m_B}^2\, {m_H}^3\, {u_H}^3\, {z_B}^2\, (z_B - z_H)\, (m_B \sin\lambda_s\, {x_B}^2\, z_B\, z_H + m_B\, u_H\, {x_B}^2\, z_B \\
&\quad - m_B \sin\lambda_s\, x_B\, x_H\, {z_B}^2 - m_B\, u_H\, x_B\, x_H\, z_B + m_H \sin\lambda_s\, x_B\, x_H\, {z_H}^2 + m_H\, u_H\, x_B\, x_H\, z_H \\
&\quad - m_H \sin\lambda_s\, {x_H}^2\, z_B\, z_H - m_H\, u_H\, {x_H}^2\, z_B))/\bar{w}^2 \\
X_4 &= g\, {m_B}^3\, {m_H}^3\, {u_H}^3\, {z_B}^3\, (x_B\, z_H - x_H\, z_B)\, (x_B - x_H)\, (z_B - z_H)/\bar{w}^3 \\
X_6 &= 0 \quad .
\end{aligned} \tag{7.5}$$

Although these expressions are complicated, they are simpler than the expressions for the same quantities in terms of the full 25-parameter Whipple model. Each of the Routh conditions (see Eqs. (4.2) & (4.3) in Chapter 4) below is necessary for self-stability. If any are not met the bicycle is not self-stable. Together they make up a sufficient condition for stability.

$A = A_0 > 0$**:** A_0 is the determinant of the positive semi-definite mass matrix. A_0 is positive when the mass matrix is non-singular. So long as both point masses are positive, the mass matrix is only singular if there exists a combination of steer and lean motions that don't move any mass. [There are two ways this can occur: 1) if the front frame mass m_H is on the steer axis so steering alone does not move any mass; or 2) if the rear frame mass m_B is on the contact line (line from rear contact point to front contact point) so leaning does not move the mass and also the front mass is off of the steering axis so that a compensating steer can keep the front mass stationary during this lean.] Thus the condition $A_0 > 0$ is generally met.

$B = B_1 v > 0$**:** For a forward moving ($v > 0$) bicycle B_1 must be positive. This occurs if a) the front mass m_H is in front of the steer axis ($u_\mathrm{H} > 0$) and the rear mass m_B is above the line connecting the rear contact point with the location of the front mass m_H, or b) the front mass m_H is behind the steer axis and the rear mass is below the line from the rear contact to the front mass.

$C = C_0 + C_2 v^2 > 0$**:** With increasing forward speed, C will be positive when C_2 is positive. This occurs if a) the front mass m_H is in front of the steer axis ($u_\mathrm{H} > 0$) and the rear mass m_B is above the front mass, or b) the front mass is behind the steer axis and the rear mass is below the front mass.

$D = D_1 v + D_3 v^3 > 0$**:** Since $D_3 = 0$ and $v > 0$, D is positive if $D_1 > 0$. This occurs if a) the front mass m_H is in front of the steer axis ($u_\mathrm{H} > 0$) and the rear-assembly mass m_B is in front of the front-assembly mass m_H or b) the front-assembly mass is behind the steer axis and the rear-assembly mass is behind the front-assembly mass.

$E = E_0 + E_2 v^2 > 0$**:** Since $E_2 = 0$, E is positive if $E_0 > 0$. This occurs a) when the front mass m_H is in front of the steer axis ($u_\mathrm{H} > 0$), and when the steer axis tilt is larger than a minimal tilt angle, that is $\lambda_\mathrm{s} > \lambda_\mathrm{s,min}$, with

$$\lambda_\mathrm{s,min} = \arctan\left(\frac{m_\mathrm{H}(x_\mathrm{H} - w)}{-m_\mathrm{B} z_\mathrm{B}}\right), \tag{7.6}$$

or b) vice versa ($u_\mathrm{H} < 0$ and $\lambda_\mathrm{s} < \lambda_\mathrm{s,min}$). The minimal steer axis tilt $\lambda_\mathrm{s,min}$ is small for a light front frame $m_\mathrm{H} << m_\mathrm{B}$ but can never be zero since $u_\mathrm{H} > 0$. Thus $(x_\mathrm{H} - w) > 0$. Thus, a theoretical two-mass-skate (TMS) bicycle with vertical steer axis can never be self-stable. Steer axis tilt (forward or backward) is necessary. Although plausible as a conjecture, this result does not hold for more general bicycles (see page 29).

$X = X_2 v^2 + X_4 v^4 + X_6 v^6 > 0$**:** Because $X_6 = 0$, with sufficiently great speed, X will become positive if X_4 is positive. This is assured if B_1, D_1, and C_2 are positive. However, the speed at which X becomes positive depends of the value of X_2, a term for which we have no simple physical interpretation.

A numerical example of a theoretical two-mass-skate (TMS) bicycle is given in Table 7.1. The eigenvalues for this theoretical TMS bicycle are shown in Figure 7.2a and the coefficients of the characteristic polynomial are shown in Figure 7.2b. The real parts of all eigenvalues are below zero for the shaded region, for forward speeds of 2.8 m/s $< v < \infty$ (Figure 7.2a).

The theoretical two-mass-skate (TMS) bicycle has zero trail. While trail is positive on common bicycles, it can be made slightly negative on the TMS bicycle without destroying its stability. However, to maintain self-stability the steer axis tilt then needs to be increased. One can further increase the stability by adding some mass moment of inertia to the front frame where one principal axis is aligned along the steer axis. These are the ingredients for the physical gyro-free stable bicycle: the experimental two-mass-skate (TMS) bicycle as described in Chapter 8.

Because the final physical design cannot be made of infinitesimal point masses, and the mass at the rear ground contact can never be located exactly at the rear contact point (it will always be slightly above), the parameters of the experimental bicycle have to be carefully chosen in order to preserve stability. All of the experimental bicycle parameters had to be fine-tuned in order to keep a stable forward speed range which starts at a low enough speed and has enough margin in the negative real part of the eigenvalues (not too close to zero) to be robust.

Another way to design a stable two-point-mass bicycle is to go through the necessary Routh conditions A–E and X but not in that order. We start with a wheelbase w, a steer axis tilt λ_s, and

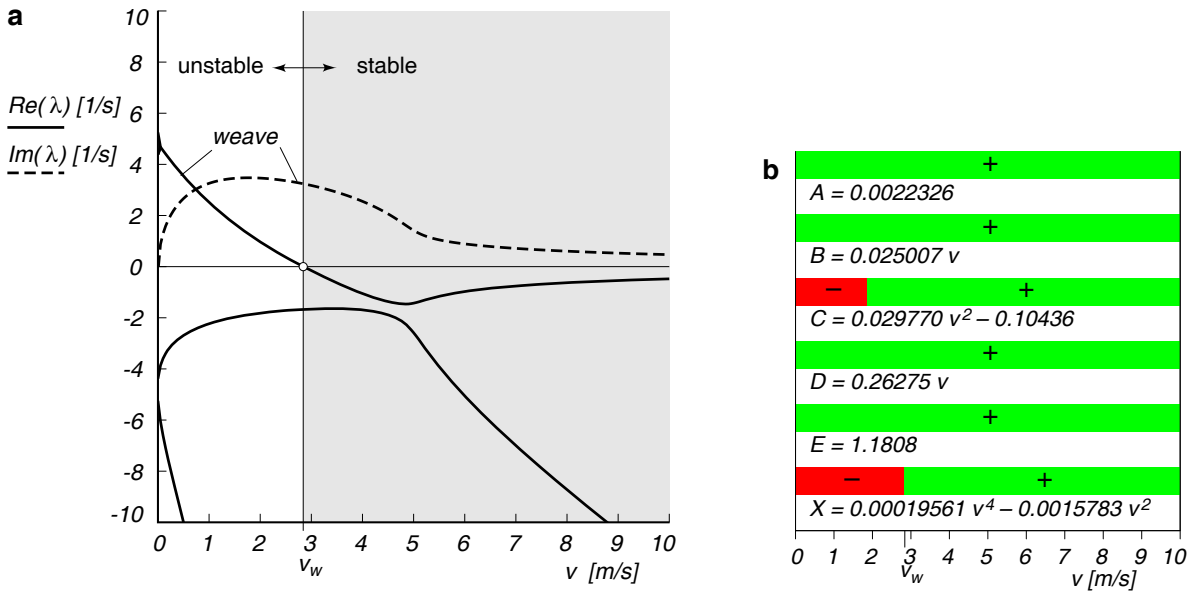

Figure 7.2: **a)** Eigenvalues and **b)** Characteristic polynomial coefficients $A \cdots X$. The bars show the speeds where the coefficients are positive (green) for a theoretical two-mass-skate (TMS) bicycle from Figure 7.1 and Table 7.1 in a forward speed range of $0 \leq v \leq 10$ m/s. Note that the real parts of all eigenvalues are negative for $v > 2.8$ m/s.

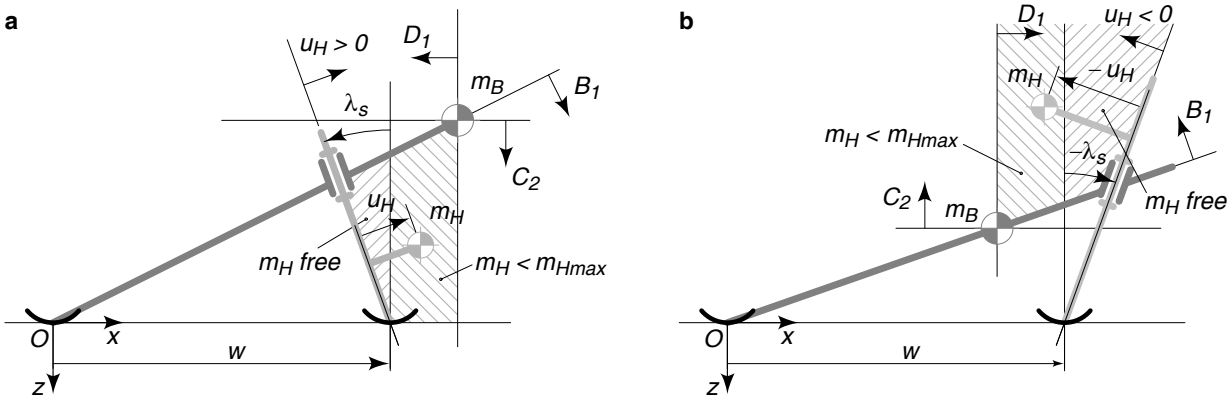

Figure 7.3: **a)** Allowed location for the front mass m_{H} (shaded areas) for which the two-point-mass bicycle to be stable when $\lambda_{\mathrm{s}} > 0$; **b)** the same but now when $\lambda_{\mathrm{s}} < 0$. The shaded regions are described in the text.

a location and value for the rear frame mass $m_{\rm B}$ and then find possible locations and values for the front mass $m_{\rm H}$. As an example we take the common case of a positive $\lambda_{\rm s}$, with leaned-back steer, see Figure 7.3a. First we use the requirement that $E_0 > 0$. E_0 is the determinant of the constant stiffness matrix $g\mathbf{K}_0$ which expands to

$$E_0 = \det(g\mathbf{K}_0) = g^2(-(m_{\rm B}\ z_{\rm B} + m_{\rm H}\ z_{\rm H})m_{\rm H}u_{\rm H}\sin\lambda_{\rm s} - m_{\rm H}^2u_{\rm H}^2).$$

Because all z-coordinates are negative, for $E_0 > 0$, we need at least $u_{\rm H}\sin\lambda_{\rm s} > 0$, and with a positive $\lambda_{\rm s}$, this means that $u_{\rm H} > 0$. In other words, for a leaned-back steer axis the front mass $m_{\rm H}$ should be in front of the steer axis. Next we apply the condition on the B coefficient, that is, $B_1 > 0$. Drawing a line from the rear contact point to the rear mass $m_{\rm B}$, we see that the front mass $m_{\rm H}$ should be below this line. Then we apply the condition on C, that is, $C_2 > 0$, by drawing a horizontal line through the rear mass $m_{\rm B}$, and see that the front mass $m_{\rm H}$ should be below this line. The next condition is on D, that is, $D_1 > 0$, which means that the front mass $m_{\rm H}$ should be behind the rear mass $m_{\rm B}$, and we draw a vertical line through $m_{\rm B}$. (Note that this makes the condition on C obsolete.) The result is the shaded area enclosed by four lines in which we can place the front mass $m_{\rm H}$. Finally we revisit the condition on E to find restrictions on the magnitude of the front mass $m_{\rm H}$. We use the expanded form of E_0 from equation (7.5),

$$E_0 = g^2m_{\rm H}u_{\rm H}\left(m_{\rm H}\left(w - x_{\rm H}\right)\cos\lambda_{\rm s} - m_{\rm B}z_{\rm B}\sin\lambda_{\rm s}\right),$$

and see that $E_0 > 0$ if $(w - x_{\rm H}) > 0$. In other words, there is no restriction on the magnitude of the front mass $m_{\rm H}$ when this mass is behind the vertical line through the front contact point within the triangular-shaped shaded region. But when $m_{\rm H}$ is in front of the vertical through the front contact point, there is a restriction on the magnitude of the front mass,

$$m_{\rm H} < m_{\rm Hmax} = m_{\rm B}\frac{-z_{\rm B}}{(x_{\rm H} - w)}\tan\lambda_{\rm s}.$$

This is in the quadrilateral shaded area next to the triangular-shaped shaded area.

The same approach can now be used but starting from a negative $\lambda_{\rm s}$, which is a forward leaned steer axis. This results in the allowed region for $m_{\rm H}$ as shown in Figure 7.3b. Note that in all cases the front mass is located in such a way that the steering in itself is unstable, or in other words, the front mass is always above the tilted steer axis, expressed here by the condition $u_{\rm H}\sin\lambda_{\rm s} > 0$. $m_{\rm Hmax}$ is inversely proportional to distance of $m_{\rm H}$ in front of the contact.

Finally, as an example, we generate an alternative theoretical two-mass-skate bicycle based on the original one from Table 7.1, but now with a forward leaned steer axis, that is $\lambda_{\rm s} \Rightarrow -\lambda_{\rm s}$. These two bicycles are drawn to scale in Figure 7.4 whereas the parameters and eigenvalues for the alternative design are shown in Table 7.2 and Figure 7.5. Note the striking similarity between the eigenvalue structure of the original theoretical two-mass-skate bicycle and the alternative design. We conjecture that by tinkering with the parameters of this alternative design we probably could get exactly the same eigenvalues as with the original design.This alternative design would have been easier to build, because the mass of the rear frame is now within the wheelbase (thus not needing a big mass near the rear contact point). But we had not thought this through at the time of construction.

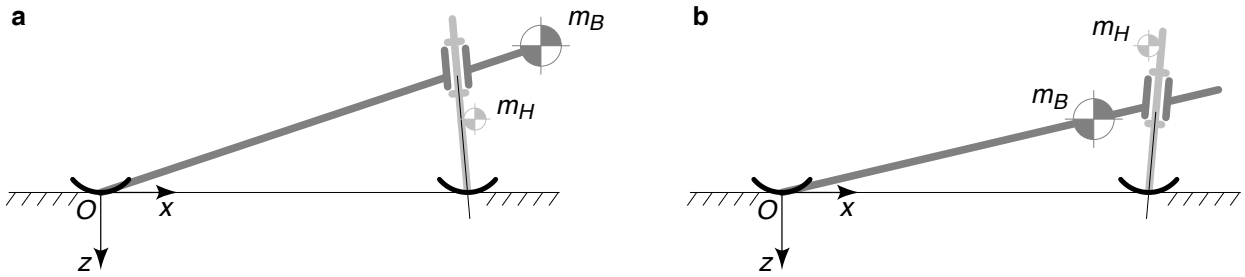

Figure 7.4: **a)** Original theoretical two-mass-skate (TMS) bicycle from Table 7.1 and **b)** alternative theoretical two-mass-skate (TMS) bicycle from Table 7.2. Both are drawn to scale.

Parameter	**Symbol**	**Value**
Wheel base	w	1 m
Steer axis tilt	λ_s	$-5°$
Rear frame assembly B mass	m_B	10 kg
Rear frame assembly B center of mass	(x_B, z_B)	$(0.85, -0.2)$ m
Front fork and handlebar assembly H mass	m_H	1 kg
Front fork and handlebar assembly H center of mass	(x_H, z_H)	$(1, -0.4)$ m

Table 7.2: Parameters for an *alternative* theoretical two-mass-skate (TMS) bicycle. Only non-zero values are mentioned.

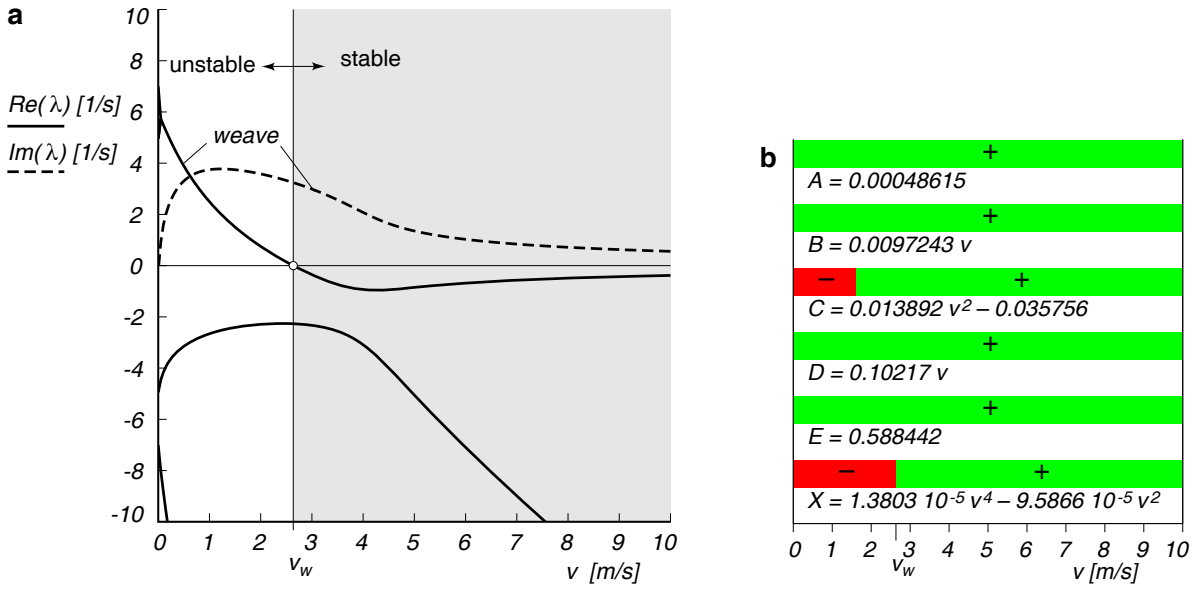

Figure 7.5: **a)** Eigenvalues and **b)** Characteristic polynomial coefficients $A \cdots X$ (green when positive) for the *alternative* theoretical two-mass-skate (TMS) bicycle from Figure 7.4b and Table 7.2 in a forward speed range of $0 \leq v \leq 10$ m/s. Note that for $v > 2.6$ m/s the real parts of all eigenvalues are negative.

Chapter 8

From theoretical two-mass-skate (TMS) bicycle to experimental TMS bicycle

To go from the infinitesimal point-mass concepts in the previous chapter to a physical design we used an iterative design process:

1. Draw a constructible bicycle in a computer aided design package (CAD, SolidWorks)
2. Export the mass, the location of the center of mass and the mass moments of inertia of the four rigid bodies of the bicycle model from this CAD model into the dynamic model.
3. Investigate how the CAD model might be adjusted such that the dynamic model has not only a stable forward speed range which starts at a low enough speed but also has enough margin in the negative real part of the eigenvalues (not too close to zero) to be robust.
4. Return to step 1.

Eventually when a physically realizable and predicted-to-be-stable model was designed in CAD, a striking similarity between the eigenvalues of the theoretical two-mass-skate (TMS) bicycle, Figure 7.2a, and the final design of the experimental TMS bicycle, in the main paper Figure 3A, was apparent.

This bicycle was then produced and all 188 parts (not counting the balls in a bearing as separate parts) – that's what it takes to connect 6 rigid objects (two wheels, two frames and two counterspinning wheels) with 5 hinges! – were weighed individually and in subassemblies. Parts/subassemblies weighing less than 10 g were weighed to an accuracy of 0.01 g, those up to 2 kg with an accuracy of 1 g and for the assemblies up to 5 kg with an accuracy of 2 g.

Independently the parts were described in a SolidWorks CAD model. The CAD program then calculated the moments of inertia and locations of centers of mass for use in the dynamics model. The total mass predicted by the CAD model differed from the measured 8837 g by less than one gram. The geometry parameters like wheelbase, steer axis tilt and location of the point masses were measured with standard mechanical hardware. A special procedure was used to measure the small negative trail, see Video 3: Measuring Trail. The parameters of the experimental TMS bicycle are shown in Table 8.1. In Table 8.2 the mass distribution across the front and rear frames is shown for the experimental TMS bicycle.

Parameter	**Symbol**	**Value for benchmark**
Wheel base	w	0.750 m
Trail	c	-0.004 m
Steer axis tilt (90° − head angle)	λ_s	7° ($90^\circ - 83^\circ$)
Gravity constant	g	9.81 N/kg
Forward speed	v	*various* m/s
Rear wheel R		
Radius	r_R	0.050 m
Mass	m_R	0 kg
Effective spin inertia	$I_{\mathrm{R}yy}$	$1.8 \cdot 10^{-5}$ kgm^2
Rear Body and frame assembly B		
Position center of mass	$(x_\mathrm{B}, z_\mathrm{B})$	$(0.5044, -0.4279)$ m
Mass	m_B	6.425 kg
Mass moments of inertia	$\begin{bmatrix} I_{\mathrm{B}xx} & 0 & I_{\mathrm{B}xz} \\ 0 & I_{\mathrm{B}yy} & 0 \\ I_{\mathrm{B}xz} & 0 & I_{\mathrm{B}zz} \end{bmatrix}$	$\begin{bmatrix} 0.875295 & 0 & 1.18665 \\ 0 & 2.59262 & 0 \\ 1.18665 & 0 & 1.73573 \end{bmatrix}$ kgm^2
Front Handlebar and fork assembly H		
Position center of mass	$(x_\mathrm{H}, z_\mathrm{H})$	$(0.7338, -0.3022)$ m
Mass	m_H	2.412 kg
Mass moments of inertia	$\begin{bmatrix} I_{\mathrm{H}xx} & 0 & I_{\mathrm{H}xz} \\ 0 & I_{\mathrm{H}yy} & 0 \\ I_{\mathrm{H}xz} & 0 & I_{\mathrm{H}zz} \end{bmatrix}$	$\begin{bmatrix} 0.038384 & 0 & -0.00055657 \\ 0 & 0.038071 & 0 \\ -0.00055657 & 0 & 0.00143206 \end{bmatrix}$ kgm^2
Front wheel F		
Radius	r_F	0.050 m
Mass	m_F	0 kg
Effective spin inertia	$I_{\mathrm{F}yy}$	$1.8 \cdot 10^{-5}$ kgm^2

Table 8.1: Parameters of the experimental two-mass-skate (TMS) bicycle (shown in Figure 2A of the main paper).

Part	**Mass** [g]
Wheels	
Rotating	174
Counter rotating	168
Total	342
Rear frame	
Point mass at front	2197
Point mass at rear contact point	2013
Supporting construction	1873
Wheels	342
Total	6425
Front frame	
Point mass	1452
Supporting contruction	618
Wheels	342
Total	2412
Total bicycle	8837

Table 8.2: Mass distribution of the experimental two-mass-skate (TMS) bicycle.

Chapter 9

Experimental two-mass-skate (TMS) bicycle construction

A photograph of the experimental TMS bicycle is shown in Figure 9.1 together with the nomenclature of the different frame parts. Here we explain some of the design choices. Based on the theory described earlier, the design we pursued has mass extending forward and above the front wheel contact. For ease of construction we gave our model a smaller wheel-base than a conventional bicycle, 0.75 m. To make non-gyroscopic wheels we added counter-rotating wheels [9, 10]. The final total mass is 8.837 kg.

The 'point' masses from the theoretical TMS bicycle model were made, for the experimental machine, of 50 mm diameter lead rods. One 1.45 kg cylinder of lead was placed 35 mm in front of and parallel to the steer axis with its center of mass 387.5 mm above the ground. Two lead cylinders, each of mass 1 kg, were each attached 100 mm above the ground to each side of the rear frame at the same longitudinal position as the rear contact point. Two 1 kg lead cylinders were connected to the carbon upper frame tube via a bracket and threaded rod 1.15 m in front and 0.90 m above the rear wheel contact point. The threaded rod allows for the compensation of miss-alignments during the assembly of the bicycle: by adjusting the mass positions to get the net center of mass in the bicycle mid-plane.

A parameter study of the location of the 2-kg mass on the front of the rear frame indicated that the fore aft position is less critical than the vertical position of the mass. Therefore a 1400 mm long upper frame tube, originating at the rear wheels is used as frame member allowing for the shallowest orientation of the beam (see Figure 9.1). On the one hand, the dynamic calculations show that stability depends on the rear frame having low inertia, on the other hand the lead cylinders require a sturdy support to ensure that no large parasitic vibrations occur. For this reason a 30 mm diameter, 1.5 mm thick carbon fiber composite tube was used for the frame material (for both the upper tube and the support tube). To further increase the ability to adjust the location of the rear frame front mass (in case the machine would not work as expected) two extra holes were drilled in the lower rear frame member (a square cross section - $30 \times 30 \times 1.5$ mm aluminum tubing), one to each side of the calculated position such that the lower end of the carbon fiber composite support tube could be placed over each of the three holes, thereby enabling the forward end of the upper frame tube to be raised or lowered by 5 cm.

The carbon tubes are connected to the aluminum lower frame by aluminum insert-brackets. The bracket-half of the insert-bracket is bolted to the the aluminum frame by a single 8 mm bolt, whilst the insert half is glued (two-component epoxy) to the inside of the carbon tube. A jig was used to align the brackets and carbon tubes during the gluing process ensuring frame symmetry. The brackets used to connect the upper shaft with the support shaft were produced using the wire electric discharging machining (EDM) method.

A crucial part of the construction of the bicycle is the'head bearing' required for steering. This

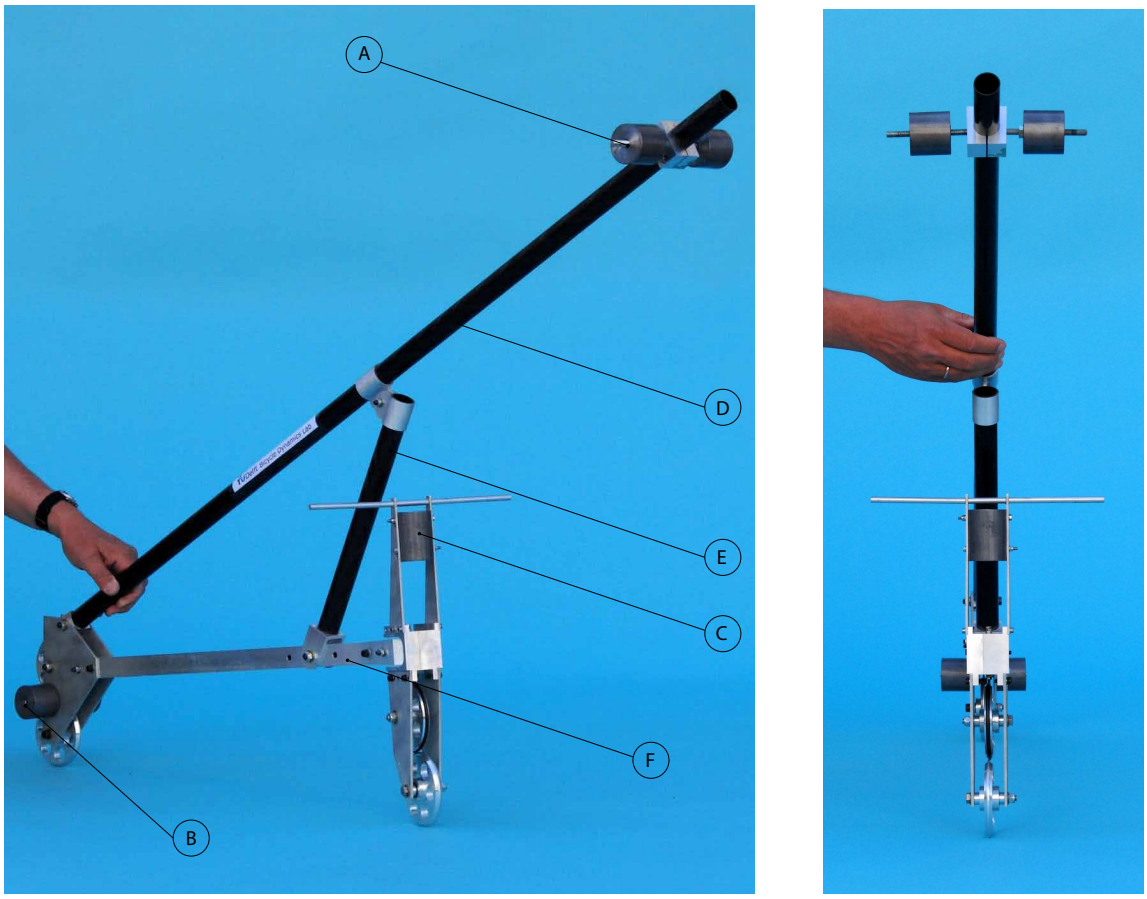

Figure 9.1: **left)** Overview of the experimental two-mass-skate bicycle, with (A) 2 kg rear frame forward point mass, (B) 2 kg point mass at the rear contact point, (C) Point mass front frame, (D) Rear frame upper tube, (E) Rear frame support tube (F) Lower rear frame member. **right)** Front view of the experimental two-mass-skate bicycle.

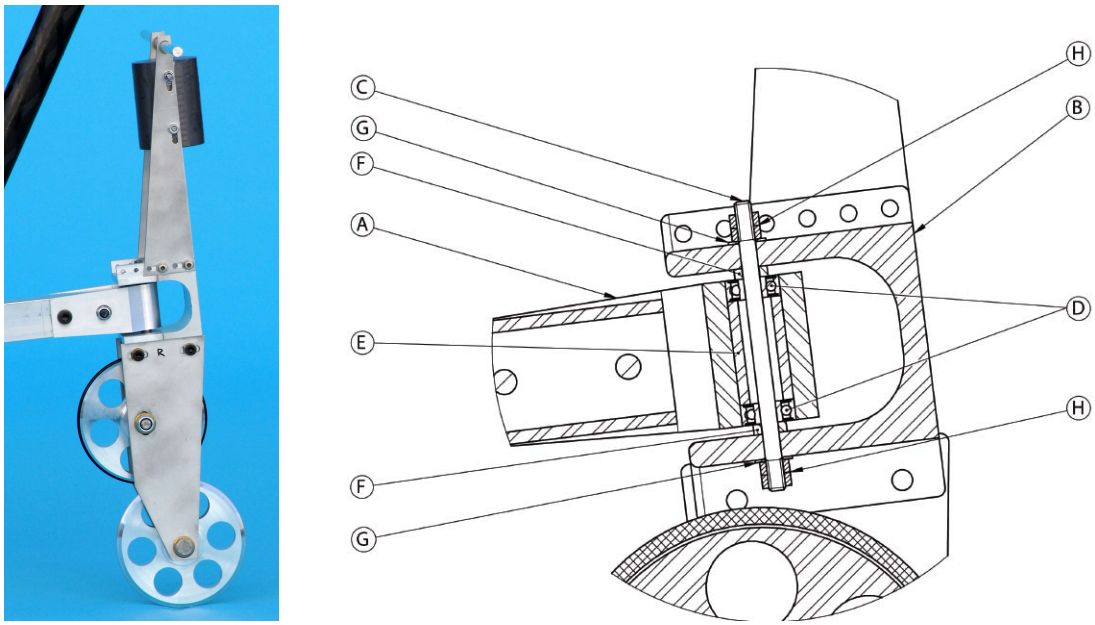

Figure 9.2: **left)** Side view of the front assembly of the experimental TMS bicycle. **right)** Front frame and steering head cross-section. (A) Rear frame head bracket, (B) Front frame head bracket, (C) Dowel with threaded ends, (D) Bearings, (E) Glued bearing spacer, (F) Spacer, (G) Washer, (H) Nuts.

'head bearing' enables relative rotations between the front frame and rear frame. Its construction details are shown Figure 9.2. We required both minimal play and minimal friction in this joint. Two small, 4 mm inner diameter, open single row deep groove ball bearings (D) were aligned by boring a hole straight through the aluminum head material (A) such that a bearing could be inserted from the top and bottom of the hole. To prevent the bearings from displacing axially, a cylinder (E), of which the outer surface was glued to the bored head, was placed between the two bearings (D). For a play-free connection between the front frame and rear frame a dowel (C) with thread on both ends was used as the axle through the bearings (D). Furthermore the two holes in the front frame head-bracket (B) were bored in one motion to ensure alignment. The gap between either side of the front frame head-bracket and the bearings was filled with a single spacer custom made to size (F). The dowel (C) was then clamped in place by nuts (H) tightened at both ends. Using small bearings (D) ensures that the arm about which the friction occurs is only roughly 4 mm, therefore minimal steering torque is required to overcome the bearing friction. As the bicycle is intended to be used only on a smooth level surface, and without a rider, the axial loads on the small bearings remain within the bearing specifications.

To achieve zero gyroscopic effect, without being restricted to ice skating rinks, the bicycle was designed with two extra wheels that counter-rotate, one relative to the front wheel and the other relative to the rear wheel [9, 10]. The addition of counter-rotating wheels eliminates the net gyroscopic effect. In the computer model, the mass properties of the set of rotating and counter-rotating wheels contribute to the masses and moments of inertia of the front and rear frame.

An important design parameter is the mass moment of inertia of the front frame about the steering axis. For self-stability this should not be too large. Therefore the counter rotating wheels had to be placed approximately in line with the steering axis. However to counteract the offset of the front frame head bracket the counter rotating wheel was placed slightly more aft as can be seen in Figure 9.2a.

A major concern was the wheel-to-ground contact. In the model, point contact is assumed. For conventional-size bicycle wheels with high-pressure pneumatic tires this has been shown to be reasonably accurate [7]. However, this model has small wheels. Initially 100 mm diameter

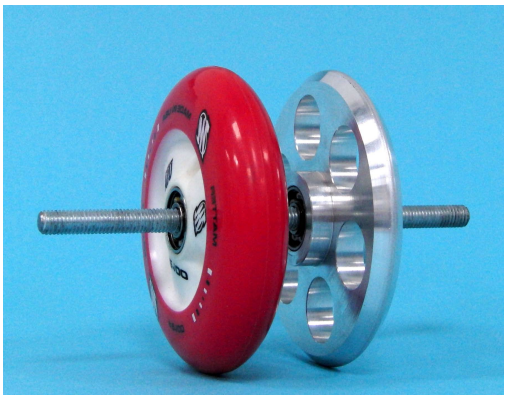

Figure 9.3: Two different types of 100 mm diameter wheels used, **left:** a polyurethane "inline skate" wheel, which didn't work, and **right:** the sharp aluminum wheel, with a crown radius of 2 mm, that was used in the experiments presented.

polyurethane wheels (sold for use on inline skates) were used (see Figure 9.3). However, with these polyurethane wheels rolling on a rubber gym floor, the experimental TMS bicycle showed no self stability. We conjecture that the large contact patch introduced a too large scrubbing torque, thereby destroying the steering dynamics. We then tried aluminum (7075-T6) wheels of 100 mm diameter, with holes drilled through to reduce the mass, see Figure 9.3. These wheels have a 2 mm crown radius shape. With these sharp hard wheels on a rubber gym floor the experimental machine did show self-stability. A defect of this design, which we never improved upon, is the low coefficient of friction between aluminum and the rubber floor. Our experiments were thus limited to small lean angles. At larger lean angles the wheels would slip laterally and cause a low-side fall.

To keep the counter-rotating wheel rotating at the same speed as the ground-contact wheel, a groove was turned into the wheel tread of the counter-rotating-wheel and a rubber O-ring was placed in this groove, thereby making the total outer diameter of the counter-rotating-wheel 100 mm once more. This rubber O-ring increased the coefficient of friction between the counter-rotating and rotating wheel.

Slotted holes in the two fork plates (both front and rear) allow the counter-rotating wheels to be displaced. By tightening the axle bolt the counter rotating wheel can be fixed in place with some pressure between the two wheels, thereby preventing slip between the wheels.

How well have we canceled the gyroscopic effects? A rough measure of the size of the gyroscopic effect of the wheels is

$$C_{\text{ang}} = \frac{\text{spin angular momentum of a wheel}}{\text{(mass of bicycle)}\cdot\text{(speed of bicycle)}\cdot\text{(height of bicycle)}} \tag{9.1}$$

$$= \frac{J\omega_{\text{wheel}}}{m_{\text{bicycle}} v h} = \frac{Jv/r_{\text{wheel}}}{m_{\text{bicycle}} v h} = \frac{J}{m_{\text{bicycle}} h r_{\text{wheel}}} \tag{9.2}$$

For a normal riderless bicycle $C_{\text{ang}} \approx 0.02$ and for our bicycle, before adding the counter-rotating wheels, $C_{\text{ang}} \approx 0.0008$. The counter-rotating wheels further reduce 90 % of even that effect. Why not 100 %? Because the counter rotating wheels have an aluminum groove cut out and an O-ring placed in the groove that is 6 g lighter. This makes the counter-rotating wheel only have 90 % of the rotary inertia of the rolling wheel. Thus our small light wheel has about 5 % the gyroscopic contribution of a normal bicycle wheel and 90 % of that is cancelled. In total our bicycle thus has about 0.5 % (one part in 200) the gyroscopic effect of a normal bicycle. At 99.5 % gyro-free, we feel comfortable saying 'no-gyro'. This could have been easily reduced to zero or less, had we thought-through before-hand that rubber O-rings have a lower density than aluminium.

Chapter 10

Experimental procedure and results

When the experimental TMS bicycle had been refined to show self-stability, at least some times, and could even be perturbed laterally without falling over, we wanted to know whether the motion was close to that predicted by the dynamic model. However, we did not want the measuring system to substantially change the mass distribution. Since mass near the rear-wheel contact point has little effect on dynamics, a wireless transmitting inertial sensor was mounted just above the rear wheel for measuring the bicycle lean and yaw. The forward speed was measured post-facto by using a high speed video camera and counting the number of frames for a fixed number of rear-wheel rotations. The wireless inertial sensor (Philips Pi-Node) measured 3-D orientation, rate of turn and acceleration.

Here are some more details about the measurements.

Forward Speed: Half of the Aluminum rear wheel was covered with black tape. A Casio Exilim EX-F1 digital photo camera was placed facing nearly perpendicular to the direction of the bicycle and used to video the motion of the bicycle with a frame rate of 300 frames per second. The launch speed of the bicycle was calculated by counting the number of frames (n_{frames}) required for the wheel to make three complete rotations as in $v = (3\pi\, 0.1)/(n_{\text{frames}}/300)$ m/s.

Lean and Yaw: A Philips Pi-Node, a wireless transmitting inertial sensor that uses 3-D accelerometers and 3-D magnetometers to provide drift free orientation data and 3 gyroscopes to track fast changes in orientation, was used. The sensor has a wireless transmitting range of 100 m. The Pi-Node upper acceleration limit is 2 g. The small amplitude, but high frequency vibrations due to the road unevenness can cause this limit to be reached, which degrades the signal. The sensor was thus taped to padding that in turn was taped on the rear frame near the rear wheel. This padding attenuated the transmission of high-frequency small amplitude vibrations to the accelerometer.

Each experiment was carried out in a gym with a rubber-like floor by two experimenters. The first experimenter worked with the bicycle, the second operated the measurement laptop computer to start and stop the data recording and operated the high-speed video camera. An experimental run starts when the collection of data on the laptop computer has started and the high speed camera is running.

The handlebars of the bicycle are initially held in the straight ahead position whilst the bicycle is brought up to speed by pushing it along in a straight line. The experimenter releases the bicycle when the bicycle feels stable. The experimenter then continues running alongside the bicycle until the lateral motions of the bicycle have mostly died out and the bicycle moves in a straight line. This is the start of the measurement. Next the bicycle is perturbed laterally by striking it (applying an impulse) on the upper (carbon fiber) frame tube, instantly giving the rear frame a lean rate. The experimenter now follows the bicycle and catches it just before it either collides with another

object (gym wall) or falls over due to the reduced speed. The bicycle is then returned to the initial location in preparation for the start of the next run. A video of such an experiment can be seen in the second run from Video 1: The Experiment.

For comparison of the experimental results with the model, first the matrix coefficients for the linearized equations of motion (3.1) were determined with the parameter values from Table 8.1 resulting in

$$\begin{aligned} \mathbf{M} &= \begin{bmatrix} 2.310172 & 0.006029 \\ 0.006029 & 0.002974 \end{bmatrix}, \qquad \mathbf{C_1} = \begin{bmatrix} 0 & 4.093917 \\ 0 & 0.027376 \end{bmatrix}, \\ \mathbf{K_0} &= \begin{bmatrix} -3.477968 & -0.033536 \\ -0.033536 & -0.004099 \end{bmatrix}, \quad \mathbf{K_2} = \begin{bmatrix} 0 & 4.602036 \\ 0 & 0.044374 \end{bmatrix}. \end{aligned} \tag{10.1}$$

The theoretical transient response of the rear frame lean angle ϕ and the steer angle δ were then calculated from the linearized equations of motion (3.1). The yaw angle of the rear frame, ψ, is a so-called ignorable coordinate and does not show up in the equations of motion. This yaw angle can be calculated from the kinematic equation,

$$\dot{\psi} = \frac{v}{w}\cos(\lambda_s)\,\delta + \frac{c}{w}\cos(\lambda_s)\,\dot{\delta}, \tag{10.2}$$

which, with substitution of the bicycle parameters from Table 8.1, is

$$\dot{\psi} = 1.3234\,v\,\delta - 0.0052936\,\dot{\delta}. \tag{10.3}$$

For the initial conditions we take the upright configuration, $\phi_0 = 0$, straight ahead, $\delta_0 = 0$. We assume that the initial steer rate is zero, $\dot{\delta}_0 = 0$. The initial lean rate, $\dot{\phi}_0$, is now the only remaining parameter. This initial condition is determined from a best fit of the measured lean rate to the simulated one. The results, the measured and simulated lean and yaw rate of the rear frame, are shown in the main paper in Figure 3B.

Chapter 11

The experiment, general observations and experiences

Physical experiments are performed in the real world, in non-ideal situations. Therefore it was envisioned that some sort of damping would be required in the wheels to compensate for the vertical unevenness of the floor and the first version of the experimental machine had 100 mm diameter polyurethane inline-skate wheels (Figure 9.3). However the bicycle fitted with these wheels seemed to have 'locked steering', presumably because of the high friction in the contact patch.

The aluminum knife-edged wheels were installed to reduce the large scrubbing torque. However, with the aluminum wheels we found performance differences that were floor dependent. The very hard wooden sports hall floors had the drawback that the surface was not continuous. The transition from one plank to the next destabilized the bicycle, occasionally tipping the bicycle or causing it to shift. The slightly softer, continuous, linoleum floor did not have the drawback of the transitions, but the coefficient of friction between the aluminum wheel and linoleum floor was so small that the smallest lateral perturbation caused the front wheel to slip away, making the bicycle fall over. The Delft University of Technology's sports center has two large sports halls with a rubber floor. The coefficient of friction between the rubber floors and the aluminum wheels were significantly larger than between the harder wooden and linoleum floors and the wheels. However sports hall number 1 has a relatively thick and soft rubber floor which significantly deforms under the bicycle wheels. The damping of this floor was so large that the bicycle reduced speed too fast to get a chance to see self-stability. The floor of sports hall number 2 was made of a thinner layer of rubber, which showed far less damping, allowing the experiments to be carried out successfully. The rolling resistance coefficient $C_\mathrm{r} = F_\mathrm{r}/(mg)$ of the wheels on the sports hall floor was calculated from the recorded video material by determining the average deceleration during the measurements. The result, $C_\mathrm{r} = 0.06$, indicates that the rolling resistance is about 10 times larger than that for conventional bicycle tires on hard pavement [35]. In summary, the wheel contact was surely far from point contact and the results are sensitive to the contact conditions. That the physical model, when it worked, corresponded well in behavior to the theoretical model could be partly fortuitous.

Lateral symmetry turned out to be a delicate issue. Because of damage and misalignments that occurred during falls, and because of padding added to prevent damaging the gym floor in the event of a fall, the bicycle was not perfectly symmetrical. We found that any small lateral symmetry offset had a large effect on the resulting stable path. A slight imbalance led to a circular path. Adjustment of the lateral position of the front masses (recall the threaded rod holding the rear frame front masses) could restore the symmetry and change the stable path back to a straight one.

Another issue is a high frequency steering oscillation that appears when the bicycle is brought

up to speed. This steering motion can clearly be seen in slow motion in Video 4, Slow Motion Experiment. This small amplitude oscillation has a frequency of roughly 20 Hertz. When the bicycle was not self stable (locked steering, polyurethane wheels, etc.) then these high frequency steering oscillation were not present.

It was not directly clear what the cause of this oscillation was so we carried out a number of tests to determine its origin. We noticed that the oscillations occur on all the floors we experimented on, and the phenomena always started at roughly walking speed. From the high speed videos that we made we determined that the oscillations have roughly the same frequency on all surfaces, about 20 Hz. The amplitude is also roughly similar (we did not measure it) on all surfaces we tested on and always settles into a limit cycle. This suggested that the cause of the oscillations could be front wheel shimmy. To investigate this we started by investigating the effect of adjusting the play about the head bearing by adjusting the nuts (H) on the dowel (C) in Figure 9.2. When the tension was decreased (play occurs in the head), no significant change was noted in the situation. However when the tension was increased and (any play remaining was removed) a small amount of pretension was placed on the head bearing, not only did the self stability of the bicycle disappear, but so did the high frequency steering oscillation indicating that it is indeed a shimmy phenomenon.

To be certain that the phenomenon really was shimmy we investigated further. Firstly we tried pressing down hard on the frame whilst pushing it along. This did not change the situation, the vibrations continued. Next we investigated the effect of the interaction between the rotating and counter-rotating wheel. First we firmly pressed the counter rotating wheel against the rotating wheel. This was done to be absolutely sure that the wheels were not slipping relative to one and other, this also made no difference to the shimmy, but did cause the bicycle to decelerate drastically. Next to be sure that any angle offset between the rotating and counter-rotating wheels causing gyroscopic steering torque was not the cause, the counter-rotating wheel was lifted slightly such that it no longer made contact with the rotating wheel so that the counter-rotating wheel no longer rotated, leaving just the ordinary situation with one rotating wheel. This made no difference to the shimmy either. Completely removing the counter-rotating wheel all together did not significantly improve the situation either. The final modification (with respect to the standard situation where both wheels were installed and the machine had straight ahead, upright, stability) that was tried was to drastically adjust the front frame's mass and inertia. We did this by removing the front frame point mass (C in Figure 9.1). This drastically changed the steering characteristics of the bicycle, which no longer showed any steering tendency and of course no self-stability, but it also completely removed the steering vibration. Thus we conclude that this high frequency oscillation is indeed shimmy and in this case of little influence on the global dynamics of the bicycle.

A final intriguing aspect that we noticed through investigating the recorded orientation data, was that directly after the perturbation the bicycle shows a yawing motion in the opposite direction (see in the main paper Figure 3B). Initially the sensor readings were doubted. However, in some of our videos the camera was positioned behind the bicycle on a skateboard that followed the bicycle from behind. This video showed that when the bicycle is struck to the left (at a high point on the frame) it starts to lean to the left, as expected. Simultaneously, however, the front wheel slips to the right causing the recording of a sudden yaw to the right, this can be seen in the second run in Video 1, The Experiment. The bicycle generally quickly recovers from this slip.

Description of videos

These are Supplementary Online Material (SOM) Videos 1–4. See authors website (on cover of this text) for links to more and higher-resolution videos and photos.

Screenshot of videos: **1)** The Experiment **2)** Counter rotating wheels **3)** Measure trail **4)** Slow Motion

Video 1 **The Experiment.** The video `Video1BasicExperiment.mp4` shows a typical experimental run. In order to effectively capture the experiment on film many different camera positions were tried. The main objective was to show that the bicycle once released follows a straight line. When it is perturbed, it stabilizes and then continues on a straight line in a new direction. The difficulty was finding a viewing position from where clearly can be seen that the bicycle actually goes through these three stages. Multiple fixed positions were tried, with both zoom and panning motions, however the most effective camera position turned out to be mobile, on a skateboard that closely followed the bicycle. One person carried out the experiment with the bicycle, the cameraman stood on the skateboard and only concentrated on filming the bicycle while a the third person pushed the cameraman forward and ensured that the distance between the bicycle and camera stayed roughly constant.

Video 2 **Counter rotating wheels.** The video `Video2CounterSpinningWheels.mp4` demonstrates the working of the front counter rotating wheel when the front wheel is rotated.

Video 3 **Measuring trail.** The video `Video3MeasuringTrail.mp4` shows how the small negative trail on the experimental two-mass-skate (TMS) bicycle is measured. A piece of paper is placed underneath the front wheel and stuck to the ground with tape. The front wheel is lowered and now touches the paper. The rear frame of the bicycle is clamped to prevent it from moving. The handlebars are then turned either way a number of times and the wheel

marks the paper. The bicycle is removed from the clamp and the mark on the paper is examined. The mark follows an arc, a line is drawn tangentially to either end of the mark. The point where the two lines cross indicates the point about which the wheel rotates. Next the arc traversed by the middle of the contact 'point' is drawn on the paper. The distance from the center point to the arc is approximately the trail. When we measured the trail this way it turned out to be -4 mm, that is, the contact point is 4 mm ahead of the intersection of the steer axis with the ground.

Video 4 **Slow motion experiment** The video `Video4SlowMotion.mp4` is a high speed video (300 fps) of one of the experiments where we measured the lateral motions with a wireless inertial sensor (Philips Pi-Node) and forward speed by post-facto counting frames.

References

The first 17 items in this reference list duplicate the references from the main paper (so as to avoid conflict where there is overlap).

[1] W. J. M. Rankine. On the dynamical principles of the motion of velocipedes. *The Engineer*, 28:79,129,153,175 and 29:2 (1870), 1869.

[2] C. Spencer. *The modern bicycle*. Frederick Warne and Co., London , 1876. (pp. 23–24).

[3] J. P. Meijaard, Jim P. Papadopoulos, Andy Ruina, and A. L. Schwab. History of thoughts about bicycle self-stability. *http://arxiv.org*, 2011.

[4] E. Carvallo. *Théorie du mouvement du monocycle et de la bicyclette.* Gauthier-Villars, Paris, France, 1899. (Submitted in 1897 for the Prix Fourneyron, awarded shared second place in 1898.).

[5] F. J. W. Whipple. The stability of the motion of a bicycle. *Quarterly Journal of Pure and Applied Mathematics*, 30:312–348, 1899. [Whipple's paper is discussed in *Nature*, Notes, 59:516-517, 30 March 1899].

[6] J. P. Meijaard, Jim M. Papadopoulos, Andy Ruina, and A. L. Schwab. Linearized dynamics equations for the balance and steer of a bicycle: a benchmark and review. *Proceedings of the Royal Society A*, 463:1955–1982, 2007.

[7] J. D. G. Kooijman, A. L. Schwab, and J. P. Meijaard. Experimental validation of a model of an uncontrolled bicycle. *Multibody System Dynamics*, 19:115–132, 2008.

[8] Ju. I. Neĭmark and N. A Fufaev. *Dynamics of nonholonomic systems.* Providence, RI: American Mathematical Society., 1972. (Transl. from the Russian edition, Nauka, Moscow, 1967.).

[9] D. E. H. Jones. The stability of the bicycle. *Physics Today*, 23(4):34–40, 1970. (reprinted in September 2006).

[10] K. J. Åström, R. E. Klein, and A. Lennartsson. Bicycle dynamics and control. *IEEE Control Systems Magazine*, 25(4):26–47, 2005.

[11] F. Klein and A. Sommerfeld. *Über die Theorie des Kreisels*. Teubner, Leipzig, 1910. Ch IX §8, Stabilität des Fahrrads, by F. Noether, pp. 863–884.

[12] J. A. Griffiths. On the Distribution of the Wheel Load in Cycles. *Proceedings of the Institution of Mechanical Engineers*, 37:128–188, 1886. (p. 162–188 discussion by C. Vernon Boys).

[13] W. T. Kelvin. *Popular Lectures and Addresses*. Macmillian and co., 1889. (pp.142–146, Kelvin's lecture of March 4, 1881).

[14] J. M. Papadopoulos. Bicycle steering dynamics and self-stability: a summary report on work in progress. Cornell Bicycle Research Project, December 1987.

[15] E. J. Routh. Stability of a dynamical system with two independent motions. *Proceedings of the London Mathematical Society*, 1(1):97, 1873.

[16] R. N. Collins. *A mathematical analysis of the stability of two wheeled vehicles*. Phd, University of Wisconsin, Madison, 1963.

[17] C.. Chateau. Vélocipédie, de laplomb dans les bicycles. *La Nature: Revue des sciences et de leurs applications aux arts et à l'industrie*, pages 353–355, 1892.

[18] F. G. Maunsell. Why does a bicycle keep upright? *Mathematical Gazette*, 30(291):195–199, 1946.

[19] M. Cook. It takes two neurons to ride a bicycle. *Demonstration at NIPS*, 4, 2004.

[20] A. van Lunteren and H. G. Stassen. On the variance of the bicycle rider's behavior. In *Proceedings of the 6th Annual Conference on Manual Control*, April 1970.

[21] D. H. Weir. *Motorcycle Handling Dynamics and Rider Control and the Effect of Design Configuration on Response and Performance*. PhD thesis, University of California, LA, 1972.

[22] A. J. R. Doyle. The essential human contribution to bicycle riding. In J. Patrick and K. Duncan, editors, *Training, human decision making, and control*, pages 351–370. North Holland, 1988.

[23] M.W. Spong. The swing up control problem for the acrobot. *IEEE Control Systems Magazine*, 15(1):49–55, 1995.

[24] W. H. Laubach. Velocipede, January 1869.

[25] Don Pardo, private communication, 2010.

[26] M. Hubbard. Lateral dynamics and stability of the skateboard. *Journal of Applied Mechanics*, 46:931–936, 1979.

[27] C. J. Cornelius. Rear-steering recumbent bicycles. *Human Power*, 8(2):6, 1990.

[28] J. W. Zellner and D. H. Weir. Development of handling test procedures for motorcycles. Technical Report 780313, SAE, 1978.

[29] R. Rice. Bicycle dynamics - simplified dynamic stability analyses. Technical Report ZN-592l-V-2, Calspan, 1976. Prepared for: Schwinn Bicycle Co.

[30] http://ruina.tam.cornell.edu/research/topics/bicycle%5Fmechanics/JBike6%5Fweb%5Ffolder/index.htm.

[31] SAE J670 (R) Vehicle Dynamics Terminology. Technical Report J670, SAE International, 2008.

[32] R. S. Hand. Comparisons and stability analysis of linearized equations of motion for a basic bicycle model. Master's thesis, Cornell University, May 1988.

[33] R. Schwarz. Accident avoidance characteristics of unconventional motorcycle configurations. Technical Report 790258, SAE, 1979.

[34] P. Gewirtz. On "I Know It When I See It". *Yale Law Journal*, 105(4), 1996.

[35] D. G. Wilson. *Bicycling Science*. The MIT Press, 3rd edition, 2004. (with contributions by J. M. Papadopoulos).